Monthly Notices
of the
ROYAL ASTRONOMICAL SOCIETY

MNRAS **451,** 126–143 (2015) doi:10.1093/mnras/stv714

Short versus long gamma-ray bursts: a comprehensive study of energetics and prompt gamma-ray correlations

Amir Shahmoradi[1]★ and Robert J. Nemiroff[2]★

[1]*Department of Physics and Institute for Fusion Studies, The University of Texas at Austin, TX 78712, USA*
[2]*Department of Physics, Michigan Technological University, Houghton, MI 49931, USA*

Accepted 2015 March 26. Received 2015 March 24; in original form 2015 January 4

ABSTRACT

We present the results of a comprehensive study of the luminosity function, energetics, prompt gamma-ray correlations, and classification methodology of short-hard and long-soft gamma-ray bursts (GRBs), based on observational data in the largest catalogue of GRBs available to this date: BATSE catalogue of 2702 GRBs. We find that (1) the least-biased classification method of GRBs into short and long, solely based on prompt-emission properties, appears to be the ratio of the observed spectral peak energy to the observed duration ($R = E_{\rm p}/T_{90}$) with the dividing line at $R \simeq 50$[keV s^{-1}]; (2) once data is carefully corrected for the effects of the detection threshold of gamma-ray instruments, the population distribution of short gamma-ray bursts (SGRBs) and long gamma-ray bursts (LGRBs) can be individually well described as multivariate lognormal distribution in the four-dimensional space of the isotropic peak gamma-ray luminosity, total isotropic gamma-ray emission, the intrinsic spectral peak energy, and the intrinsic duration; (3) relatively large fractions of SGRBs and LGRBs with moderate-to-low spectral peak energies have been missed by BATSE detectors; (4) relatively strong and highly significant intrinsic hardness–brightness and duration–brightness correlations likely exist in both populations of SGRBs and LGRBs, once data is corrected for selection effects. The strengths of these correlations are very similar in both populations, implying similar mechanisms at work in both GRB classes, leading to the emergence of these prompt gamma-ray correlations.

Key words: methods: analytical – methods: numerical – methods: statistical – gamma-ray burst: general.

1 INTRODUCTION

The field of gamma-ray bursts (GRBs) has witnessed rapid growth over the past decades, in particular, following the launches of NASA *Compton Gamma-Ray Observatory* (Meegan et al. 1992), *Swift* (Gehrels et al. 2004), and *Fermi* (Michelson, Atwood & Ritz 2010) missions. Early hints to the existence of distinct populations of gamma-ray transients (e.g. Mazets et al. 1981; Norris et al. 1984), and at least two classes of short-hard (Type-I) and long-soft (Type-II) GRBs (Dezalay et al. 1992) have now been extensively corroborated and confirmed by the prompt-emission data from independent gamma-ray detector missions (e.g. Kouveliotou et al. 1993; Gehrels, Ramirez-Ruiz & Fox 2009; Zhang et al. 2012a) or follow-up observations of the afterglows or host galaxies (e.g. Zhang et al. 2009; Berger 2011, 2014). Although the possibility of more than two classes of GRBs with distinct progenitors has been extensively discussed and considered (e.g. Horvath 1998; Mukherjee et al. 1998; Balastegui, Ruiz-Lapuente & Canal 2001; Hakkila et al. 2001, 2004; Gehrels et al. 2006; Horvath et al. 2006, 2008, 2012; Chattopadhyay et al. 2007; Virgili, Liang & Zhang 2009; Gao, Lu & Zhang 2010; Kóbori et al. 2014; Levan et al. 2014), it has remained a matter of debate and speculation to this date (e.g. Hakkila et al. 2000a,b,c, 2003a, 2004; Shahmoradi 2013b; Levan et al. 2014; Zhang et al. 2014).

Beginning with the influential work of Kouveliotou et al. (1993), GRBs have been traditionally classified into two populations of short and long GRBs (SGRBs and LGRBs, respectively) based on a sharp cut-off on the bimodal distribution of the observed duration (T_{90}) of prompt gamma-ray emission, generally set to $T_{90} \sim 2$–3[s]. Nevertheless, the detector and energy dependence of the observed GRB duration (e.g. Fenimore et al. 1995; Nemiroff 2000; Qin et al. 2013) has prompted many studies in search of alternative less-biased methods of GRB classification, typically based on a combination of the prompt gamma-ray emission and/or afterglow/host properties (e.g. Gehrels, Ramirez-Ruiz & Fox 2009; Zhang et al. 2009, 2012a; Goldstein, Preece & Briggs 2010; Lü et al. 2010, 2014; Shahmoradi & Nemiroff 2011; Zhang, Chen & Huang 2012b; Shahmoradi 2013b) or using the prompt-emission spectral correlations in

★ E-mail: amir@physics.utexas.edu (AS); nemiroff@mtu.edu (RJN)

conjunction with the traditional method of classification (e.g. Qin & Chen 2013).

Ideally, a phenomenological classification method of GRBs should be based on their intrinsic (i.e. rest-frame) properties, free from potential biases due to data analysis, detector specifications, observational selection effects, and sample incompleteness. Such method is currently far from reach due to detector-induced heterogeneity in available GRB catalogues (e.g. Qin et al. 2013) and complex selection effects in the detection, analysis, and redshift measurement processes (e.g. Hakkila et al. 2000b, 2003a; Band & Preece 2005; Nakar & Piran 2005; Butler et al. 2007; Nava et al. 2008; Butler, Kocevski & Bloom 2009; Shahmoradi & Nemiroff 2009, 2011; Butler, Bloom & Poznanski 2010; Coward et al. 2013; Shahmoradi 2013a,b, cf. Shahmoradi & Nemiroff 2011 for a comprehensive review of relevant literature).

Historically, the intrinsic properties of SGRBs have also been less studied compared to LGRBs, potentially due to lack of redshift information for the majority of SGRBs (e.g. Coward et al. 2012). This has led to an additional obstacle towards a quantitative GRB taxonomy. While the population properties of LGRBs and their progenitors have been extensively researched and fairly well constrained (e.g. Dainotti, Ostrowski & Willingale 2011; Dainotti et al. 2013, 2015; Lien et al. 2013, 2014; Shahmoradi 2013a,b; Howell et al. 2014; Littlejohns & Butler 2014; Pescalli et al. 2015, cf. Shahmoradi 2013 for a comprehensive review of the literature), the cosmic rate and the intrinsic prompt-emission properties of SGRBs are far less understood and investigated (e.g. Guetta, Piran & Waxman 2005; Guetta & Piran 2006; Nakar, Gal-Yam & Fox 2006; Salvaterra et al. 2008; Chapman, Priddey & Tanvir 2009; Czerny et al. 2011; Virgili et al. 2011; Wanderman & Piran 2015).

Motivated by the existing gap and uncertainties in the current knowledge of the intrinsic population properties of SGRBs and the lack of an efficient, quantitative, bias-free classification method for GRBs into long and short subgroups, here we present a methodology and model to constrain the energetics, luminosity function and the joint distributions and correlations of the prompt gamma-ray emission of SGRBs. Despite lacking a complete knowledge of the true cosmic rate and redshift distribution, here we argue and show that SGRBs exhibit very similar prompt-emission correlations and population distribution to those of LGRBs as presented by Shahmoradi (2013b), both qualitatively and, under plausible cosmic rate assumptions, also quantitatively. This result, along with other recent works on the time-resolved and time-integrated spectral properties of SGRBs (e.g. Ghirlanda et al. 2011; Shahmoradi & Nemiroff 2011; Zhang et al. 2012b; Tsutsui et al. 2013; Calderone et al. 2015) points towards the possibility of a unified mechanism responsible for the prompt gamma-ray emission of the two GRB classes, independently of the diverse progenitor candidates for the two GRB populations.

This work also paves the way towards a detector-independent minimally biased phenomenological classification method for GRBs solely based on the observed prompt gamma-ray data of individual events. Towards this, we focus our attention on the largest sample of uniformly detected GRBs to this date: the BATSE catalogue of 2702 GRBs (Paciesas et al. 1999; Goldstein et al. 2013). In the following sections, we present an example of data mining on BATSE data that showcases the tremendous amount of useful, yet unexplored information buried in this seemingly archaic GRB catalogue.

We devote Section 2.1 of this manuscript to presenting an elaborate method of classification for the *observed* sample of GRBs into two subclasses of short-hard and long-soft GRBs. In Section 2.2, we elaborate on the construction of a GRB world model that is capable of describing BATSE SGRB data. This is followed by a discussion of the procedure for fitting the model to BATSE data in Section 2.4. The predictions of the model together with univariate and multivariate goodness-of-fit (GoF) tests are presented in Section 3, followed by a discussion of the similarities and differences in the population distributions of SGRBs and LGRBs in Section 4. The main findings of the presented GRB world model are summarized in Section 5.

2 GRB WORLD MODEL

2.1 Sample selection

Depending on the triggering criteria, some gamma-ray detectors facilitate the detection of one class of bursts over the others (e.g. Paciesas et al. 1999; Band 2003, 2006; Hakkila et al. 2003b; Band et al. 2008; Lien et al. 2014). For example, the specific detector sensitivity of the Burst Alert Telescope (BAT) onboard *Swift* satellite results in better detections of LGRBs over SGRBs (e.g. Band 2003, 2006). Compared to BAT however, BATSE Large Area Detectors (LADs) had an increased *relative* sensitivity to SGRBs (e.g. Band 2003; Hakkila et al. 2003b). Several studies have already offered new methods for a global detector-independent phenomenological classification of GRBs based on empirical relations that are believed to hold for only a specific class of GRBs or based on the prompt or afterglow emission data (e.g. Zhang et al. 2009; Lü et al. 2010; Qin & Chen 2013). These methods however, either suffer from sample incompleteness or require information, such as redshift, that might not be available for the majority of GRBs (e.g. Coward et al. 2012, 2013).

Here in this work, we ensure a minimally biased analysis of short-duration class of GRBs by following the classification approach of Shahmoradi (2013b), which to the extent of our knowledge provides the least-biased classification of BATSE GRBs, solely based on prompt emission data[1]. The word 'bias' here refers to the systematic contamination of data and analysis that might be introduced when using the traditional definition of GRB classes, based on a sharp cut-off on the duration variable T_{90} (Kouveliotou et al. 1993), as it is generally used by many GRB researchers (e.g. Guetta et al. 2005; Butler et al. 2010; Campisi, Li & Jakobsson 2010; Wanderman & Piran 2010).

The classification method used here is based on fuzzy C-means clustering algorithm of Dunn (1973), Bezdek (1981): each BATSE GRB is assigned a probability (i.e. class coefficient) of belonging to LGRB (versus SGRB) population, the value of which depends on the set of GRB variables used in classification. This can be any combinations of the peak flux (P_{50-300} [photon s^{-1} cm^{-2}]) in BATSE detection energy range [50–300 keV], in three different time-scales – 64, 256, and 1024 [ms], bolometric fluence (S_{bol} [erg cm^{-2}]), the observer-frame spectral peak energy (E_p [keV]), for which we use estimates by Shahmoradi & Nemiroff (2010), and the observed duration (T_{90} [s]).[2] Then, GRBs with LGRB class coefficient >0.5 are flagged as long-duration bursts. Following Shahmoradi (2013b), we

[1] The authors have already investigated multiple classification methodologies, on a variety of GRB characteristics, that are documented in Shahmoradi & Nemiroff (2011) and Shahmoradi (2013b).

[2] All BATSE GRB data are taken from the current BATSE catalogue and the spectral peak energies (E_p) are taken from Shahmoradi & Nemiroff (2010), publicly available at https://sites.google.com/site/amshportal/research/aca/in-the-news/lgrb-world-model.

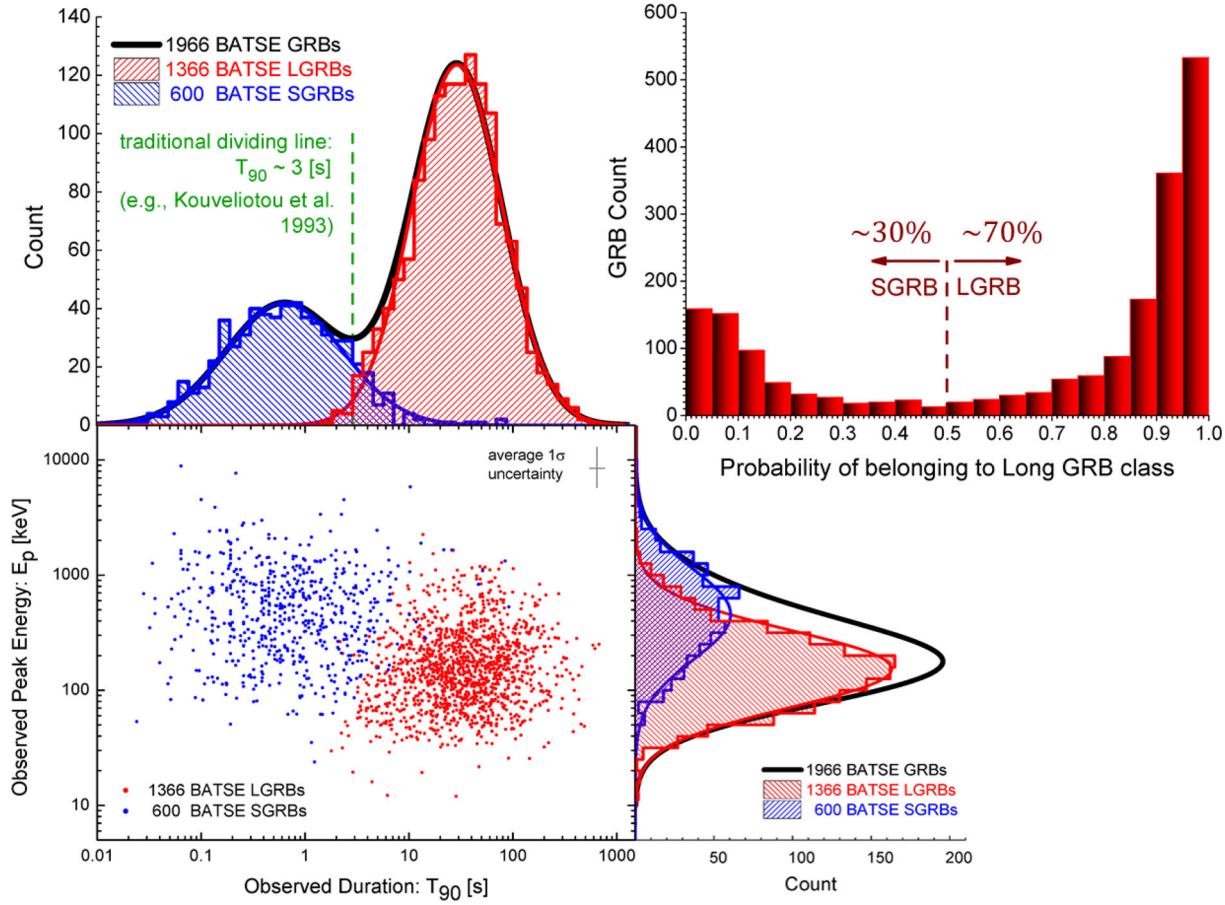

Figure 1. Classification of 1966 BATSE GRBs with measured peak flux (P_{bol}), fluence (S_{bol}), and observed duration (T_{90}) taken from the current BATSE catalogue and measured spectral peak energies (E_p) taken from Shahmoradi & Nemiroff (2010). The segregation methodology is based on fuzzy C-means clustering algorithm using the two GRB variables E_p and T_{90} that are least affected by the triggering threshold of the BATSE LADs (cf. Section 2).

make use of only two GRB variables E_p and T_{90} for classification of the sample into long and short GRBs. Unlike E_p and T_{90} which are weakly coupled to (i.e. correlated with) the variable peak flux (P_{bol}), the population distribution of the two other GRB prompt variables (S_{bol} and P_{bol}) are strongly affected by the detector threshold and not suitable for classifications based on fuzzy C-means algorithms. This is mainly due to the sensitivity of C-means clustering method to different subgroup sizes, orientations, and asymmetries (cf. Shahmoradi 2013b, section 2.1 and appendix A therein for details). In addition, the two GRB populations are most distinctively separated in the plane of T_{90}–E_p. This classification led to the initial selection of 1366 events as LGRBs and 600 events as SGRBs in our sample of 1966 BATSE GRBs with complete prompt emission data as illustrated in Fig. 1, also in Section 2.1 of Shahmoradi (2013b).

To ensure minimal contamination of the two GRB classes, the light curves of 291 bursts among 1966 BATSE GRBs with SGRB class coefficients in the range of 0.3–0.7 were also visually inspected in the four main energy channels of BATSE LADs. This led to reclassification of some events as soft gamma repeaters or from one class to another, thus reducing the size of the original SGRB sample to 565 (Table 1).[3] Shahmoradi (2013b) finds that the inclusion of the uncertainties on the two GRB variables T_{90} and E_p has marginal effects on the derived samples of the two GRB classes discussed above. Also, a classification based on T_{50} instead of T_{90} resulted in about the same sample sizes for the two GRB classes with a minimal difference of ∼0.7 per cent (cf. Section 2.1, appendix A, and fig. 1 in Shahmoradi 2013b for further comparison and details of different classification methods).

2.2 Model construction

Our primary goal in this work is to derive a multivariate statistical model that, subject to BATSE detection threshold, is capable of reproducing the observational data of 565 BATSE SGRBs. Examples of multivariate treatment of GRB luminosity function and energetics are rare in studies of GRBs. Conversely, many authors have focused primarily on the univariate distribution of the spectral parameters, most importantly on the luminosity function. This is particularly true for the short population of GRBs where the prompt, afterglow, and redshift information of individual events are scarcely available. In Shahmoradi (2013b) we argued that an accurate modelling of the luminosity function of LGRBs requires at least two GRB observable incorporated in the model: the bolometric peak flux (P_{bol}) and the observed peak energy (E_p). The parameter E_p is required,

[3] It is notable that the same simulation protocol for the original 600 BATSE events flagged as SGRBs did not result in any qualitative change in the conclusions of this work, although the strength and significance of the measured parameters of the model are affected by the presence of potential non-SGRB events in data.

Table 1. BATSE catalogue GRB trigger numbers classified as SGRBs.

Trigger	Trigger	Trigger	Trigger	Trigger	Trigger	Trigger	Trigger	Trigger	Trigger	Trigger	Trigger	Trigger	Trigger
108	138	185	207	218	229	254	289	297	373	432	474	480	486
491	508	512	537	547	551	555	568	575	603	677	729	734	788
799	809	830	834	836	845	856	867	878	906	909	929	936	942
974	1051	1073	1076	1088	1096	1097	1102	1112	1128	1129	1154	1211	1223
1289	1308	1346	1359	1404	1435	1443	1453	1461	1481	1518	1546	1553	1566
1588	1634	1635	1636	1637	1659	1662	1665	1679	1680	1683	1694	1719	1736
1741	1747	1760	1851	1953	1968	2003	2037	2040	2041	2043	2044	2049	2056
2068	2099	2103	2115	2117	2125	2126	2132	2142	2145	2146	2155	2159	2161
2163	2167	2201	2205	2206	2217	2220	2265	2268	2273	2283	2288	2312	2326
2327	2330	2332	2352	2353	2357	2358	2360	2365	2368	2372	2377	2382	2384
2395	2401	2424	2434	2448	2449	2454	2485	2487	2502	2504	2512	2513	2523
2529	2536	2564	2583	2585	2597	2599	2614	2615	2623	2632	2633	2649	2679
2680	2690	2693	2701	2715	2728	2748	2755	2757	2760	2776	2788	2795	2799
2800	2801	2810	2814	2821	2823	2828	2834	2844	2846	2849	2851	2860	2861
2873	2879	2892	2894	2910	2918	2933	2952	2964	2966	2973	2975	2977	2978
2987	2988	2995	3016	3027	3037	3038	3039	3043	3051	3066	3073	3078	3087
3094	3113	3114	3118	3121	3137	3144	3146	3152	3155	3160	3164	3173	3215
3218	3266	3278	3280	3282	3286	3293	3294	3297	3308	3323	3333	3335	3338
3340	3342	3349	3359	3374	3379	3384	3437	3441	3476	3477	3487	3494	3502
3510	3530	3545	3606	3611	3640	3642	3665	3668	3722	3728	3735	3737	3742
3751	3770	3774	3782	3791	3799	3810	3866	3867	3868	3888	3889	3894	3895
3902	3904	3910	3919	3921	3936	3939	3940	4327	4660	4744	4776	4807	4871
4955	5079	5206	5212	5277	5339	5439	5448	5453	5456	5458	5459	5461	5467
5469	5471	5485	5488	5491	5498	5499	5500	5501	5527	5528	5529	5533	5536
5537	5546	5547	5556	5560	5562	5564	5576	5592	5599	5607	5619	5620	5633
5638	5647	5650	5664	5724	5730	5733	5740	5770	5992	6091	6096	6105	6117
6120	6123	6135	6136	6145	6153	6166	6178	6180	6182	6204	6205	6215	6216
6219	6230	6237	6238	6251	6263	6265	6275	6281	6284	6292	6299	6301	6307
6314	6331	6338	6341	6342	6343	6347	6354	6361	6368	6372	6376	6385	6386
6398	6401	6411	6412	6427	6436	6439	6443	6445	6447	6452	6462	6469	6486
6488	6497	6535	6540	6542	6543	6547	6562	6569	6571	6573	6579	6580	6586
6591	6606	6634	6635	6638	6641	6643	6645	6659	6662	6671	6679	6682	6689
6693	6697	6700	6710	6715	6718	6753	6757	6786	6787	6788	6800	6824	6866
6867	6870	6904	6916	6931	7009	7060	7063	7078	7102	7106	7133	7142	7148
7159	7173	7187	7227	7240	7281	7283	7287	7290	7292	7294	7297	7305	7329
7344	7353	7359	7361	7366	7367	7375	7378	7427	7430	7440	7447	7449	7453
7455	7456	7472	7495	7496	7508	7514	7526	7547	7554	7559	7581	7584	7595
7599	7601	7602	7626	7663	7671	7706	7710	7734	7745	7753	7754	7775	7784
7789	7793	7800	7805	7827	7830	7901	7912	7922	7939	7943	7952	7970	7979
7980	7988	7995	7999	8018	8027	8035	8041	8047	8072	8076	8077	8079	8082
8085	8089	8097	8104	8120	–	–	–	–	–	–	–	–	–

since most gamma-ray detectors are photon counters, a quantity that depends on not only $P_{\rm bol}$ but also $E_{\rm p}$ of the burst. This leads to the requirement of using a bivariate distribution as the minimum acceptable model for LGRBs, for the purpose of constraining the luminosity function.

For the class of SGRBs, the duration distribution (e.g. T_{90}) of the population spans a wide range from milliseconds to tens of seconds. The wide duration distribution is particularly important in modelling BATSE LADs, since SGRBs could be potentially triggered on any of three triggering time-scales: 64, 256, and 1024 ms. Therefore, an SGRB world model should minimally incorporate the joint *trivariate* distribution of $P_{\rm bol}$, $E_{\rm p}$ and an appropriate definition of the observed duration (e.g. T_{90}). The duration variable is required in order to correctly account for the detection threshold of BATSE LADs. In addition, the definition of the observer-frame parameter *bolometric peak flux* ($P_{\rm bol}$) and the corresponding rest-frame parameter $L_{\rm iso}$ merits special attention in the study of SGRBs. Here we use the 64 ms definition of peak flux, $P_{\rm bol,\,64}$, for SGRBs taken from BATSE catalogue data, in contrast to the two other common definitions: 256 and 1024 ms. Unlike the case for LGRBs (e.g. Shahmoradi 2013b), we show in the addendum to this article (Appendix A and B) that $P_{\rm bol,64}$ is the least-biased measure of peak flux for the majority of BATSE SGRBs, also the best definition for an appropriate modelling of the BATSE detection threshold in the case of SGRBs.

Hereafter in the text and figures, the two parameters $P_{\rm bol}$ and $L_{\rm iso}$ implicitly refer to a 64 ms definition of peak flux and luminosity wherever used for SGRBs and to the commonly used 1024 ms definitions wherever used for LGRBs.

Following the arguments of Shahmoradi (2013b) for LGRBs, we propose the multivariate lognormal distribution as the simplest natural candidate model capable of describing BATSE SGRB data. The motivation behind this choice of model comes from the available observational data that closely resembles a joint multivariate lognormal distribution for four most widely studied temporal and spectral parameters of both GRB classes in the observer frame: $P_{\rm bol}$, $S_{\rm bol}$ (bolometric fluence), $E_{\rm p}$, T_{90}. Since most SGRBs are expected to originate from low redshifts $z \lesssim 3$, the convolution of these

observer-frame parameters with the redshift distribution results in negligible variation in the shape of the rest-frame joint distribution of the same SGRB parameters. Therefore, the redshift-convoluted four-dimensional (4D) rest-frame distribution can be well approximated as a linear translation of the observer-frame parameters to the rest-frame parameter space, keeping the shape of the distribution almost intact (e.g. Balazs et al. 2003). This implies that the joint distribution of the intrinsic SGRB variables – the isotropic peak luminosity ($L_{\rm iso}$), the total isotropic emission ($E_{\rm iso}$), the rest-frame time-integrated spectral peak energy ($E_{\rm p,z}$), and the rest-frame duration ($T_{90,z}$) – might be indeed well described as a multivariate lognormal distribution.

We model the process of SGRB observation as a non-homogeneous Poisson process whose mean rate parameter – the cosmic SGRB differential rate, $\mathcal{R}_{\rm cosmic}$ – is the product of the differential comoving SGRB rate density $\dot{\zeta}(z)$ with a $p=4$ dimensional lognormal probability density function (pdf), $\mathcal{LN}$, of four SGRB variables – $L_{\rm iso}$, $E_{\rm iso}$, $E_{\rm p,z}$, and $T_{90,z}$ – with location vector $\boldsymbol{\mu}$ and the scale (i.e. covariance) matrix $\boldsymbol{\Sigma}$,

$$\mathcal{R}_{\rm cosmic} = \frac{{\rm d}N}{{\rm d}L_{\rm iso}\,{\rm d}E_{\rm iso}\,{\rm d}E_{\rm p,z}\,{\rm d}T_{90,z}\,{\rm d}z}$$
$$\propto \mathcal{LN}\left(L_{\rm iso}, E_{\rm iso}, E_{\rm p,z}, T_{90,z}|\boldsymbol{\mu}, \Sigma\right)\frac{\dot{\zeta}(z)\frac{{\rm d}V}{{\rm d}z}}{(1+z)}, \quad (1)$$

where $\dot{\zeta}(z)$ is the comoving SGRB rate density, and the factor $(1+z)$ in the denominator accounts for cosmological time dilation. The comoving volume element per unit redshift, $\frac{{\rm d}V}{{\rm d}z}$, is given by,

$$\frac{{\rm d}V}{{\rm d}z} = \frac{C}{H_0}\frac{4\pi {D_{\rm L}}^2(z)}{(1+z)^2[\Omega_{\rm M}(1+z)^3+\Omega_\Lambda]^{1/2}}, \quad (2)$$

with $D_{\rm L}$ standing for the luminosity distance,

$$D_{\rm L}(z) = \frac{C}{H_0}(1+z)\int_0^z {\rm d}z'[(1+z')^3\Omega_{\rm M}+\Omega_\Lambda]^{-1/2}, \quad (3)$$

assuming a flat Λ cold dark matter cosmology, with parameters set to $h=0.70$, $\Omega_{\rm M}=0.27$, and $\Omega_\Lambda=0.73$ (Jarosik et al. 2011) for consistency with the work of Shahmoradi (2013b). The parameters C and $H_0=100\,h\,[{\rm km\,s^{-1}\,Mpc^{-1}}]$ stand for the speed of light and the Hubble constant, respectively.

The four-dimensional lognormal distribution of equation (1), $\mathcal{LN}$, has an intimate connection to the multivariate Gaussian distribution in the logarithmic space of SGRB observable parameters (cf. appendix D in Shahmoradi 2013b).

Finally, in order to obtain the observed rate ($\mathcal{R}_{\rm obs}$) of SGRBs detected by BATSE LADs, the cosmic SGRB rate, $\mathcal{R}_{\rm cosmic}$, in equation (1) must be convolved with an accurate model of BATSE trigger efficiency for SGRBs, η,

$$\mathcal{R}_{\rm obs} = \eta(L_{\rm iso}, E_{\rm p,z}, T_{90,z}, z)\times\mathcal{R}_{\rm cosmic}. \quad (4)$$

In reality, the variable η is a highly complex function of observational conditions and prompt emission characteristics, almost unique to each individual GRB. Nevertheless, we show in Appendix A that it can be approximated as a generic function of the burst's redshift (z), isotropic luminosity ($L_{\rm iso}$), the rest-frame spectral peak energy ($E_{\rm p,z}$), and the rest-frame duration ($T_{90,z}$).

2.3 The SGRB rate density

The largest source of uncertainty in population studies of SGRBs originates from the lack of an accurate knowledge of their cosmic rate. Only a small fraction of heterogeneously detected SGRBs have measured redshifts to this date (e.g. Coward et al. 2012) and redshift completeness often limits studies to the brightest events (e.g. D'Avanzo et al. 2014). It is therefore, perceivable that the current observed redshift distribution of SGRBs is likely strongly biased and not representative of the entire population of SGRBs (e.g. Nakar 2007; Coward et al. 2013). An alternative approach to empirical determination of the rate of SGRBs is through population synthesis simulations (e.g. Belczynski et al. 2006), based on the assumption of 'compact binary mergers' as the progenitor of the majority of SGRBs (e.g. Paczynski 1986; Eichler et al. 1989; Narayan, Paczynski & Piran 1992). In this scenario, the cosmic rate of SGRBs follows the star formation rate (SFR) convolved with a distribution of the *delay time* between the formation of a binary system and its coalescence due to gravitational radiation.

There is currently no consensus on the statistical moments and shape of the delay time distribution, solely based on observations of individual events and their host galaxies. The median delays vary widely in the range of ∼0.1–7 Gyr depending on the assumptions involved in estimation methods or in the dominant binary formation channels considered (e.g. Belczynski et al. 2006; Hopman et al. 2006; Berger et al. 2007; Bogomazov, Lipunov & Tutukov 2007; Zheng & Ramirez-Ruiz 2007; Berger 2011; Hao & Yuan 2013; Guelbenzu et al. 2014). Recent results from population synthesis simulations however, favour very short delay times of a few hundred million years with a long negligible tail towards several billion years (e.g. O'Shaughnessy, Belczynski & Kalogera 2008; Belczynski et al. 2010).

The computational expenses and limitations imposed on this work strongly limit the number of possible scenarios that could be considered for the cosmic rate of SGRBs. Thus, in order to approximate the comoving rate density $\dot{\zeta}(z)$ of SGRBs, we adopt the SFR of Hopkins & Beacom (2006) in the form of a piecewise power-law function,

$$\mathcal{SFR}(z)\propto\begin{cases}(1+z)^{\gamma_0} & z<z_0\\ (1+z)^{\gamma_1} & z_0<z<z_1\\ (1+z)^{\gamma_2} & z>z_1,\end{cases} \quad (5)$$

with parameters $(z_0, z_1, \gamma_0, \gamma_1, \gamma_2)$ set to the best-fitting values (0.993, 3.8, 3.3, 0.055, −4.46) of an updated SFR fit by Li (2008). The SFR is then convolved with a lognormal model of the delay time distribution (e.g. Nakar 2007),

$$\mathcal{LN}(\tau|\mu,\sigma)\propto\frac{1}{\tau\sigma}{\rm e}^{-\frac{(\ln\tau-\mu)^2}{2\sigma^2}}, \quad (6)$$

with parameters $[\mu,\sigma]=[\log(0.1), 1.12]$ in units of billion years (Gyr) estimated from the population synthesis simulation results of (e.g. Belczynski et al. 2010), such that the comoving rate density of SGRBs is calculated as,

$$\dot{\zeta}(z)\propto\int_z^\infty \mathcal{SFR}(z')\mathcal{LN}(t(z)-t(z'))\frac{{\rm d}t}{{\rm d}z'}{\rm d}z', \quad (7)$$

with the Universe's age $t(z)$ at redshift z given by,

$$t(z)=\frac{1}{H_0}\int_z^\infty\frac{{\rm d}z'}{(1+z')\sqrt{(1+z')^3\Omega_{\rm M}+\Omega_\Lambda}}. \quad (8)$$

We also fit data with alternative cosmic rates of SGRBs, assuming that SGRBs follow SFR of Hopkins & Beacom (2006) or the convolution of SFR with a long merger delay time of lognormal form with parameters $[\mu,\sigma]=[\log(4.0\,{\rm Gyr}), 0.3]$ as suggested by Nakar (2007). For all redshift scenarios, we find that the resulting best-fitting parameters are qualitatively the same, although some

parameters may exhibit quantitative differences at $>1\sigma$ significance level.

2.4 Model fitting

Now, with a statistical model at hand for the observed rate of SGRBs (i.e. equation 4), we proceed to obtain the best-fitting parameters of the model to BATSE SGRBs data. In principle, any model fitting must take into account the observational uncertainties and any prior knowledge from independent sources, which can be achieved via Bayesian multilevel methodology (e.g. Hobson et al. 2010). This is done by first constructing the likelihood function, taking into account the uncertainties in observational data (e.g. Loredo 2004): Under the assumption of symmetric Gaussian uncertainties, as it is the case with BATSE catalogue data, the full Poisson likelihood of data $\boldsymbol{\mathcal{O}}$ given the parameters $\{\boldsymbol{\mu}, \Sigma\}$ of the SGRB world model in equations (1) and (4) can be written as,

$$\mathcal{L}(\boldsymbol{\mathcal{O}} \mid \boldsymbol{\mu}, \Sigma) = \mathcal{A}^N \exp\left(-\mathcal{A}\int_{\boldsymbol{O}\text{space}} \mathcal{R}_{\rm obs}(\boldsymbol{O} \mid \boldsymbol{\mu}, \Sigma, \eta)\, \mathrm{d}\boldsymbol{O}\right)$$

$$\times \prod_{i=1}^{565} \int_{\boldsymbol{O}\text{space}} \mathcal{R}_{\rm cosmic}(\boldsymbol{O} \mid \boldsymbol{\mu}, \Sigma)\mathcal{L}_i(\boldsymbol{O} \mid \hat{\boldsymbol{O}}(\boldsymbol{\mu}_i, \Sigma_i))\, d\boldsymbol{O}, \qquad (9)$$

in which $\mathcal{A}$ is a factor that properly normalizes the cosmic rate of SGRBs ($\mathcal{R}_{\rm cosmic}$) and the vector $\hat{\boldsymbol{O}}(\boldsymbol{\mu}_i, \Sigma_i)$, standing for the ith SGRB Observation in BATSE catalogue, has the likelihood $\mathcal{L}_i$ of having the true parameters $\boldsymbol{O} \equiv [L_{\rm iso}, E_{\rm iso}, E_{\rm p,z}, T_{90,z}]$ in the rest-frame four-dimensional observation space ($\boldsymbol{O}$space) that can be described as a Gaussian pdf with parameters $\{\boldsymbol{\mu}_i, \Sigma_i\}$ obtained from BATSE catalogue such that,

$$\mathcal{L}_i(\boldsymbol{O}) \sim \mathcal{N}(\boldsymbol{O}|\boldsymbol{\mu}_i, \Sigma_i). \qquad (10)$$

In this sense, the term $\mathcal{R}_{\rm cosmic}$ in equation (9) acts as a Bayesian prior for $\mathcal{L}_i$. In the absence of this prior knowledge however, as it is the case with BATSE SGRBs, the empirical Bayes approach provides an alternative solution, in which an ad hoc estimate of the model parameters $\{\boldsymbol{\mu}, \Sigma\}$ based on the observed data – excluding uncertainties – serves as the prior for the same data – including uncertainties – at the second level of analysis (e.g. Hobson et al. 2010). The joint posterior of the unknown parameters of the model can be then written as,

$$\mathcal{P}(\boldsymbol{\mu}, \Sigma|\boldsymbol{\mathcal{O}}) \propto \mathcal{P}(\boldsymbol{\mu}, \Sigma) \times \mathcal{L}(\boldsymbol{\mathcal{O}}|\boldsymbol{\mu}, \Sigma). \qquad (11)$$

As for the choice of *hyperprior*, $\mathcal{P}(\boldsymbol{\mu}, \Sigma)$, we adopt the non-informative uniform prior for the mean vector $\boldsymbol{\mu}$. A variety of non-informative or weakly informative priors for the covariance matrix $\boldsymbol{\Sigma}$ have been already proposed and considered in the literature, with inverse Wishart family of distributions among the most popular choices (cf. John Barnard 2000 and references therein). Here, to avoid problems and complications associated with inverse Wishart priors, we adopt a separation strategy (e.g. Browne 2006) by decomposing the covariance matrix $\boldsymbol{\Sigma}$ into a correlation matrix and a set of standard deviations. We then use uniform priors on the log-transformation of all standard deviations, also on the Fisher transformation (Fisher 1915) of all correlation coefficients.

Due to the complex truncation imposed on SGRB data and the world model by BATSE detection threshold (cf. Appendix A), maximization of the likelihood function of equation (9) is analytically intractable. Calculation of the normalization factor $\mathcal{A}$ by itself requires a multivariate integral over the four-dimensional space of SGRB variables at any given redshift. In addition, due to lack of redshift (z) information for BATSE SGRBs, the probability for observation of each SGRB given the model parameters must be marginalized over all possible redshifts. These numerical integrations make sampling from the posterior distribution of equation (11) an extremely difficult task. Given the potential presence of unknown systematic biases in BATSE catalogue data as discussed in Appendix B, (also by Koshut et al. 1996; Hakkila et al. 2000b, 2003a; Shahmoradi 2013b, Appendix C) and the high level of uncertainty in the redshift distribution of SGRBs, we take a bold but reasonable and highly simplifying step and drop data uncertainties in the calculation of the likelihood function (equation 9) in order to bring the problem into the realm of current computational technologies. The joint posterior distribution of the model parameters is then obtained by iterative sampling using a variant of Markov Chain Monte Carlo (MCMC) techniques known as Adaptive Metropolis-Hastings (e.g. Haario, Saksman & Tamminen 2001). To further the efficiency of MCMC sampling, we implement all algorithms in FORTRAN (Backus 1978; Metcalf, Reid & Cohen 2011) and approximate the numerical integration in the definition of the luminosity distance of equation (3) by the analytical expressions of Wickramasinghe & Ukwatta (2010). This integration is encountered on the order of billion times during MCMC sampling from the posterior distribution (cf. appendix C in Shahmoradi 2013b for further details of the MCMC sampling method).[4]

3 RESULTS AND GOODNESS-OF-FIT TESTS

The resulting *mean* and 1σ standard deviations of the model parameters are tabulated in Table 2. It is notable that the parameters of the model exhibit strong covariance as illustrated in the upper triangle (above the bold values) of the correlation matrix of Table 3. For comparison, the lower triangle of the table represents the correlation matrix of the same parameters for the LGRB world model based on 1366 BATSE LGRBs (table 3 in Shahmoradi 2013b). All location parameters of the model appear to strongly correlate with each other, so do the scale parameters. The correlations among the four variables of the world models also weaken with increasing the location parameters. Therefore, given BATSE data, a higher cosmic rate of LGRBs and SGRBs at high redshifts generally implies weaker correlations among the prompt gamma-ray emission variables, in particular, the brightness–hardness type of relations. A comparison of the predicted redshift distribution of BATSE SGRBs with LGRBs is illustrated in the *left-hand plot* of Fig. 2.

The lack of redshift information combined with the relatively small sample size of BATSE GRBs strongly limit the variety of GoF tests that can be employed to assess the performance of the model. In addition to small sample size, marginalization of the likelihood function (equation 9) over redshift variable, and the systematic biases in data close to detection threshold (cf. Appendix B), have major contributions to the uncertainties of the best-fitting parameters of the model (Table 2) and increase the risk of overfitting. Following Shahmoradi (2013b), the fitting results can be first visually inspected by superposing the univariate distribution of four variables of the SGRB world model on BATSE data, as illustrated in Fig. 3. For comparison, the results of LGRB world model fit to BATSE LGRB data from Shahmoradi (2013b) are also shown by the red-colour lines and histograms.

[4] The entire simulation codes and algorithms will be available for download at https://github.com/shahmoradi/grb_world.

Table 2. Mean best-fitting parameters of SGRB world model, compared to LGRB world model of Shahmoradi (2013b).

Parameter	SGRB world model	LGRB world model
	Redshift parameters (equation 5)	
z_0	0.993	0.993
z_1	3.8	3.8
γ_0	3.3	3.3
γ_1	0.0549	0.0549
γ_2	−4.46	−4.46
	Lognormal merger delay (equation 6)	
$\mu_{\rm delay}$	0.1	–
$\sigma_{\rm delay}$	1.12	–
	Location parameters	
$\log(L_{\rm iso})$	51.88 ± 0.16	51.54 ± 0.18
$\log(E_{\rm iso})$	50.93 ± 0.19	51.98 ± 0.18
$\log(E_{{\rm p},z})$	2.98 ± 0.05	2.48 ± 0.05
$\log(T_{90,z})$	-0.74 ± 0.08	1.12 ± 0.03
	Scale parameters	
$\log(\sigma_{L_{\rm iso}})$	-0.36 ± 0.06	-0.25 ± 0.06
$\log(\sigma_{E_{\rm iso}})$	-0.10 ± 0.04	-0.08 ± 0.03
$\log(\sigma_{E_{{\rm p},z}})$	-0.39 ± 0.02	-0.44 ± 0.02
$\log(\sigma_{T_{90,z}})$	-0.24 ± 0.02	-0.37 ± 0.01
	Correlation coefficients	
$\rho_{L_{\rm iso}-E_{\rm iso}}$	0.91 ± 0.03	0.94 ± 0.01
$\rho_{L_{\rm iso}-E_{{\rm p},z}}$	0.51 ± 0.10	0.45 ± 0.07
$\rho_{L_{\rm iso}-T_{90,z}}$	0.50 ± 0.09	0.48 ± 0.09
$\rho_{E_{\rm iso}-E_{{\rm p},z}}$	0.60 ± 0.06	0.58 ± 0.04
$\rho_{E_{\rm iso}-T_{90,z}}$	0.63 ± 0.05	0.60 ± 0.05
$\rho_{E_{{\rm p},z}-T_{90,z}}$	0.12 ± 0.06	0.31 ± 0.04
	BATSE detection efficiency (equation A5)	
$\mu_{\rm thresh}$	-0.25 ± 0.03	-0.45 ± 0.02
$\log(\sigma_{\rm thresh})$	-0.86 ± 0.05	-0.90 ± 0.05

Note. The full Markov Chain sampling of the above parameters from the 16-dimensional parameter space of the likelihood function are available for download at https://sites.google.com/site/amshportal/research/aca/in-the-news/lgrb-world-model for the LGRB world model and at https://github.com/shahmoradi/grb_world for SGRBs world model.

At the second level of GoF tests, the joint bivariate distributions of pairs of GRB variables can be compared to model predictions as illustrated in Figs 4, 5, 6. The trace of BATSE trigger threshold on the populations of both SGRBs and LGRBs is visible in most bivariate distribution plots. Following Shahmoradi (2013b) and in order to ensure a good fit to the joint bivariate distributions of the four prompt emission parameters of SGRBs, we also compare the model predictions with observational data along the principal axes of the bivariate distributions, as depicted in the *centre and bottom* plots of Figs 4, 5, 6. Although, statistically not a sufficient test for *multivariate* GoF of the model to observational data, this comparison can provide strong evidence in favour of or against a good fit, at much higher confidence than solely comparing the model predictions and data via marginal distributions, as illustrated in Fig. 3.

A comparison of the bivariate model predictions with data along the principal axes immediately reveals the potential systematic biases that exist in BATSE catalogue data close to detection threshold (e.g. *centre-right and bottom-left* plots of Fig. 4). We show in Appendix B that this bias has its origins primarily in the duration (T_{90}) and peak photon flux ($P_{\rm bol}$) measurements of BATSE GRBs.

This method of scanning the model and data along the principal axes of the joint bivariate distributions can be generalized to trivariate and quadruvariate joint distributions. For brevity, however, only the bivariate tests are presented here.

4 DISCUSSION

Throughout previous sections, we presented and explained an elaborate analysis to constrain the energetics, luminosity function, and the prompt gamma-ray correlations of SGRBs, subject to detection threshold of gamma-ray detectors, here BATSE LADs. The methodology employed in this work is similar to the LGRB population study of Shahmoradi (2013b). We have argued and shown that the intrinsic population distributions of both long and short GRBs can be well described by a multivariate lognormal model in the four-dimensional prompt gamma-ray emission parameter space of the isotropic peak luminosity ($L_{\rm iso}$), total isotropic emission ($E_{\rm iso}$), the spectral peak energy ($E_{{\rm p},z}$), and the prompt duration ($T_{90,z}$). This was done by first employing a fuzzy clustering method to segregate the BATSE catalogue GRBs into long and short classes (Section 2.1), followed by a careful modelling of the effects of the BATSE detection threshold on the two GRB populations (Appendix A).

Ideally, if the population properties of both SGRBs and LGRBs can be well described by multivariate lognormal distribution as argued in Section 2.2, also by Shahmoradi (2013a) and Shahmoradi (2013b), then a multivariate lognormal *mixture* model ought to be used in order to simultaneously fit for the distributions of the entire BATSE catalogue of LGRBs and SGRBs together. Therefore, the classification of the observed sample prior to model fitting as performed in Section 2.1 would be unnecessary and the members of the two GRB populations would be automatically determined by the best-fitting parameters of the mixture model. Nevertheless, our experimentation with mixture models generally led to either degenerate or very poor fitting results for BATSE GRB data. This is primarily due to the morphological differences in the light curves and spectra of short and long GRBs, which in turn result in challenging difficulties in modelling the BATSE triggering algorithm in a unified framework for both GRB classes in the multivariate mixture model.

In the following sections, we discuss the key findings of the presented work and compare the results with data and findings from other gamma-ray experiments and population studies of GRBs.

4.1 Luminosity function and isotropic emission

Despite being an ill-defined quantity, the isotropic peak luminosity ($L_{\rm iso}$) is among the most widely used and investigated parameters of the prompt emission of GRBs. The vague and conventional definition of $L_{\rm iso}$ stems from its dependence on the time-scale used to define this quantity, commonly set to $t = 1024\,{\rm ms} \sim 1$ [sec] ($L_{\rm iso,\,1024\,ms}$). Although the $L_{\rm iso,1024\,ms}$ definition of the peak luminosity is more or less independent of the duration (e.g. $T_{90,z}$) of the long class of GRBs, it is strongly duration-dependent for the class of SGRBs (Fig. A1). This is primarily due to the diverse range of prompt durations of SGRBs, with many of the detected bursts lasting only a fraction of a second. Alternative definitions of the peak luminosity have been already proposed in order to provide

Table 3. Correlation matrix of the parameters of the SGRB world model. For comparison, the correlation matrix of the LGRB world for a cosmic rate following SFR of Li (2008) is reported in the lower triangle below the bold values of the table (cf. Shahmoradi 2013b).

Parameter	$\log(L_{iso})$	$\log(E_{iso})$	$\log(E_{p^{\prime}z})$	$\log(T_{90^{\prime}z})$	$\log(\sigma_{L_{iso}})$	$\log(\sigma_{E_{iso}})$	$\log(\sigma_{E_{p^{\prime}z}})$	$\log(\sigma_{T_{90^{\prime}z}})$	$\rho_{L_{iso}-E_{iso}}$	$\rho_{L_{iso}-E_{p^{\prime}z}}$	$\rho_{L_{iso}-T_{90^{\prime}z}}$	$\rho_{E_{iso}-E_{p^{\prime}z}}$	$\rho_{E_{iso}-T_{90^{\prime}z}}$	$\rho_{E_{p^{\prime}z}-T_{90^{\prime}z}}$	μ_{thresh}	$\log(\sigma_{thresh})$
$\log(L_{iso})$	1.00	0.95	0.59	0.77	-0.87	-0.78	-0.28	-0.42	-0.17	0.04	-0.16	-0.04	-0.25	-0.27	-0.49	-0.26
$\log(E_{iso})$	0.96	1.00	0.66	0.83	-0.88	-0.86	-0.33	-0.48	-0.33	-0.05	-0.27	-0.11	-0.33	-0.35	-0.47	-0.25
$\log(E_{p^{\prime}z})$	0.88	0.90	1.00	0.43	-0.62	-0.70	-0.58	-0.23	-0.43	-0.67	-0.10	-0.71	-0.09	-0.52	-0.28	-0.16
$\log(T_{90^{\prime}z})$	0.34	0.43	0.39	1.00	-0.71	-0.76	-0.22	-0.67	-0.40	0.06	-0.61	0.05	-0.64	-0.33	-0.35	-0.17
$\log(\sigma_{L_{iso}})$	-0.90	-0.90	-0.81	-0.35	1.00	0.90	0.36	0.40	0.27	0.06	0.19	0.18	0.25	0.39	0.32	0.15
$\log(\sigma_{E_{iso}})$	-0.85	-0.89	-0.83	-0.52	0.94	1.00	0.48	0.51	0.58	0.25	0.41	0.33	0.41	0.56	0.26	0.12
$\log(\sigma_{E_{p^{\prime}z}})$	-0.56	-0.60	-0.78	-0.32	0.57	0.66	1.00	0.10	0.36	0.60	0.05	0.64	-0.04	0.27	0.17	0.11
$\log(\sigma_{T_{90^{\prime}z}})$	-0.13	-0.14	-0.13	-0.20	0.13	0.18	0.10	1.00	0.23	-0.05	0.42	-0.09	0.55	0.20	0.16	0.08
$\rho_{L_{iso}-E_{iso}}$	-0.00	-0.10	-0.17	-0.52	0.01	0.31	0.31	-0.02	1.00	0.47	0.58	0.37	0.32	0.41	0.00	-0.01
$\rho_{L_{iso}-E_{p^{\prime}z}}$	-0.45	-0.50	-0.74	-0.32	0.48	0.60	0.83	0.08	0.43	1.00	-0.01	0.92	-0.13	0.36	0.00	0.03
$\rho_{L_{iso}-T_{90^{\prime}z}}$	0.42	0.35	0.31	-0.56	-0.45	-0.22	-0.14	0.01	0.59	-0.05	1.00	-0.04	0.89	0.46	-0.04	-0.06
$\rho_{E_{iso}-E_{p^{\prime}z}}$	-0.49	-0.54	-0.76	-0.33	0.54	0.65	0.84	0.09	0.36	0.96	-0.10	1.00	-0.13	0.54	0.01	0.01
$\rho_{E_{iso}-T_{90^{\prime}z}}$	0.41	0.35	0.33	-0.55	-0.44	-0.26	-0.19	0.11	0.38	-0.14	0.95	-0.16	1.00	0.54	0.02	-0.02
$\rho_{E_{p^{\prime}z}-T_{90^{\prime}z}}$	0.01	-0.05	-0.01	-0.59	0.05	0.20	0.04	0.13	0.35	0.04	0.61	0.15	0.66	1.00	0.00	-0.04
μ_{thresh}	-0.66	-0.64	-0.59	-0.19	0.49	0.44	0.34	0.08	-0.06	0.24	-0.26	0.26	0.24	-0.06	1.00	0.74
$\log(\sigma_{thresh})$	-0.42	-0.41	-0.38	-0.11	0.29	0.26	0.21	0.05	-0.05	0.15	-0.16	0.16	-0.15	-0.05	0.78	1.00

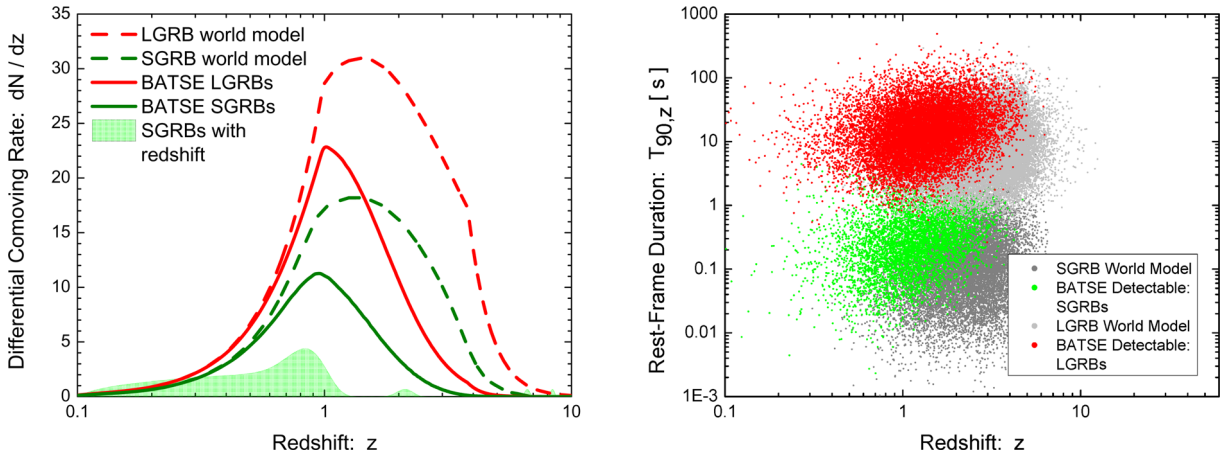

Figure 2. Left: The predicted redshift distribution of BATSE SGRBs and LGRBs. The green-coloured histogram represents the sample of SGRBs with known redshift taken from Tsutsui et al. (2013). Assuming an average merger delay time of ∼0.1Gyrs (e.g. Belczynski et al. 2010), about 60 per cent of BATSE SGRBs originate from redshifts $z \gtrsim 1.0$, highlighting the potential existence of strong selection effects in redshift measurements of SGRBs. **Right:** The intrinsic duration distribution of LGRBs and SGRBs versus redshift. Corroborating the independent findings of Littlejohns & Butler (2014) based on *Swift* data, the presented GRB world model predicts that the shortest duration LGRBs & SGRBs at high redshifts generally have the lowest likelihood of detection by gamma-ray instruments such as BATSE LAD, *Fermi* GBM and *Swift* BAT detectors.

a universal definition of the peak luminosity, independent of the duration and type of the burst, such as the *effective luminosity* definition of Butler et al. (2010). Nevertheless, such global luminosity definitions cannot be employed in the presented analysis due to the specific triggering algorithm of BATSE LADs, which is defined for three distinct fixed time-scales: 64, 256, and 1024 ms. Therefore, in order to minimize the effects of GRB duration on the definition of peak luminosity, we have used the highest resolution time-scale (64 ms) for the definition of the isotropic peak luminosity of BATSE SGRBs. By contrast, the one-second peak luminosity ($L_{\rm iso,1024\,ms}$) is sufficiently accurate and almost independent of the prompt duration of almost all LGRBs, whether detected or undetected (cf. Shahmoradi 2013b).

Given BATSE SGRB data, we find a 3σ range of $\log(L_{\rm iso}{\rm erg\,s^{-1}}) \in [50.0, 53.0]$ for the distribution of the 64-ms peak luminosities of SGRBs. Depending on the burst duration from long to short, the

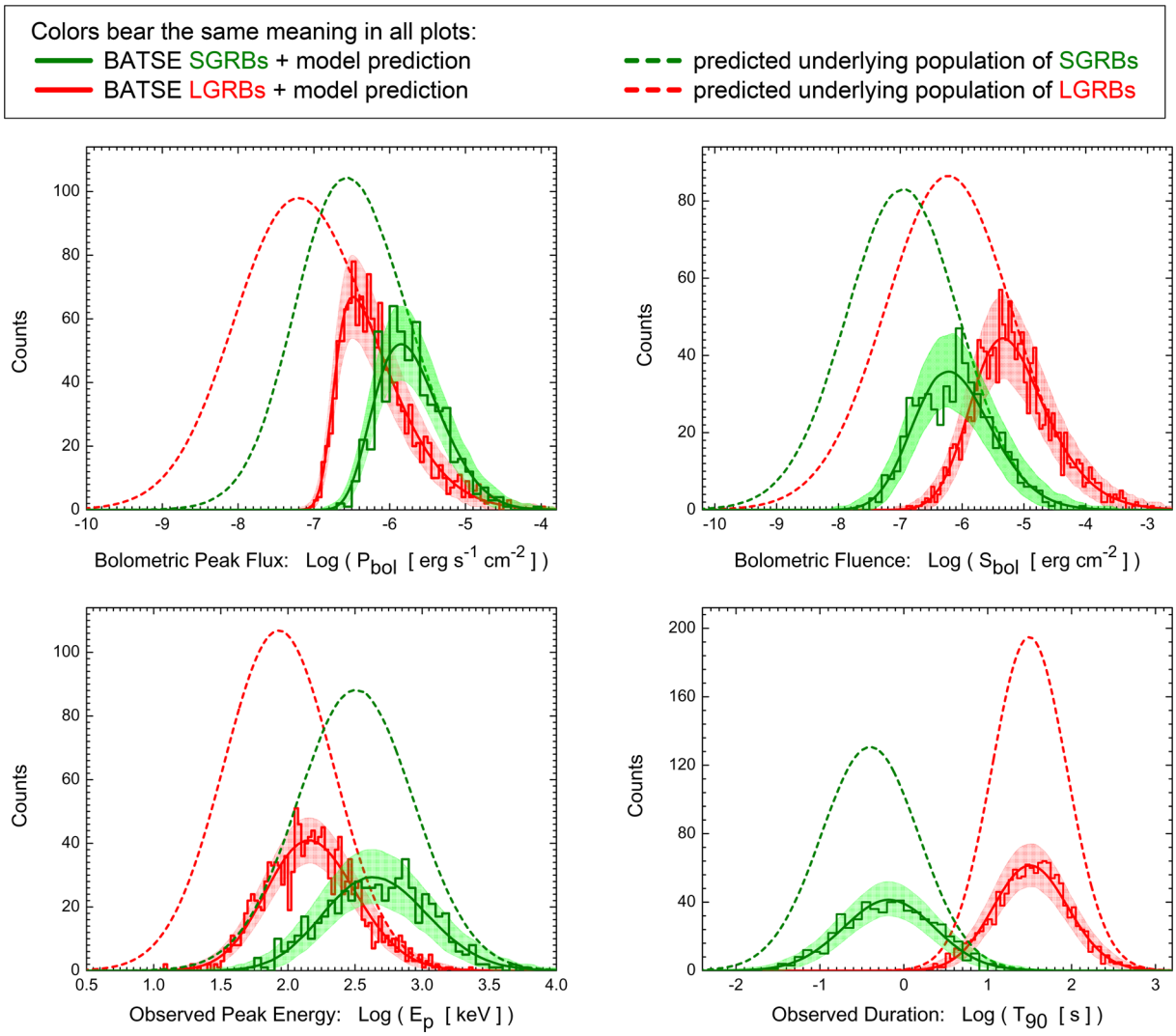

Figure 3. Univariate predictions of the *multivariate* best-fitting SGRB and LGRB world models for BATSE catalogue GRBs. The red and green colours represent data and model for SGRBs and LGRBs, respectively. Each plot illustrates the projection of the multivariate GRB world model (*solid curves*) on the distribution of one of the four prompt gamma-ray emission variables (red and green *histograms*): peak flux $P_{\rm bol}$, fluence $S_{\rm bol}$, observed peak energy $E_{\rm p}$, and the observed duration T_{90}, subject to BATSE detection threshold. The colour-shaded areas represent the 90 per cent prediction intervals of the model for BATSE data. The *dashed lines* represent the predicted underlying populations of LGRBs and SGRBs, respectively. Fitting results for LGRBs are taken from Shahmoradi (2013b). For clarity, the bin size for SGRB histograms and data is twice as large as the bin size for LGRBs histograms and data in all plots.

64-ms peak luminosity of SGRBs can be on average 1.5 to 13 times larger than the conventional 1024-ms time-scale definition of the peak luminosity, commonly used for LGRBs. Knowing that the most luminous bursts generally tend to be the longest, we obtain a conservative range of $\log(L_{\rm iso,1024\,ms}{\rm erg\,s^{-1}}) \in [48.9, 53.1]$ for SGRBs. For comparison, Shahmoradi (2013b) finds a 3σ range of $\log(L_{\rm iso}{\rm erg\,s^{-1}}) \in [49.5, 53.5]$ for the population of LGRBs.

It should be noted however, that the prompt-emission GRB quantities, in particular, the isotropic peak luminosity and the cosmic rates of GRBs are very sensitive to the detection threshold of the specific detector used to collect observational data, and to the systematic biases in measurements close to detection threshold (cf. Appendix B). This has also been noted in an earlier study of the population properties of *Swift* LGRBs by Butler et al. (2010).

As for the population distribution of the total isotropic emission of SGRBs, we obtain a 3σ range of $\log(E_{\rm iso}\,{\rm erg}) \in [48.0, 53.5]$. For comparison, a 3σ range of $\log(E_{\rm iso}\,{\rm erg}) \in [49.2, 54.7]$ was obtained for LGRBs by Shahmoradi (2013b). Therefore, it appears that LGRBs are on average more than one order of magnitude brighter than SGRBs. It is however, notable that the width of the distribution of $E_{\rm iso}$ is approximately the same in both populations of LGRBs and SGRBs. The same also holds for the width of the distribution of $L_{\rm iso}$ in the two GRB classes.

4.2 Spectral peak energy and prompt duration

The spectral peak energies of SGRBs have long been observed to be systematically higher than the typical peak energies of the class of LGRBs (e.g. Kouveliotou et al. 1993). The extent and significance of the difference between the two populations however, has remained a matter of speculation due to sample incompleteness and unknown selection biases in observational data of both GRB classes. The methodology presented in this work enabled us for the first time to set stringent constraints on the potential underlying *population* distribution of the spectral peak energies of both GRB classes in both observer and rest frames.

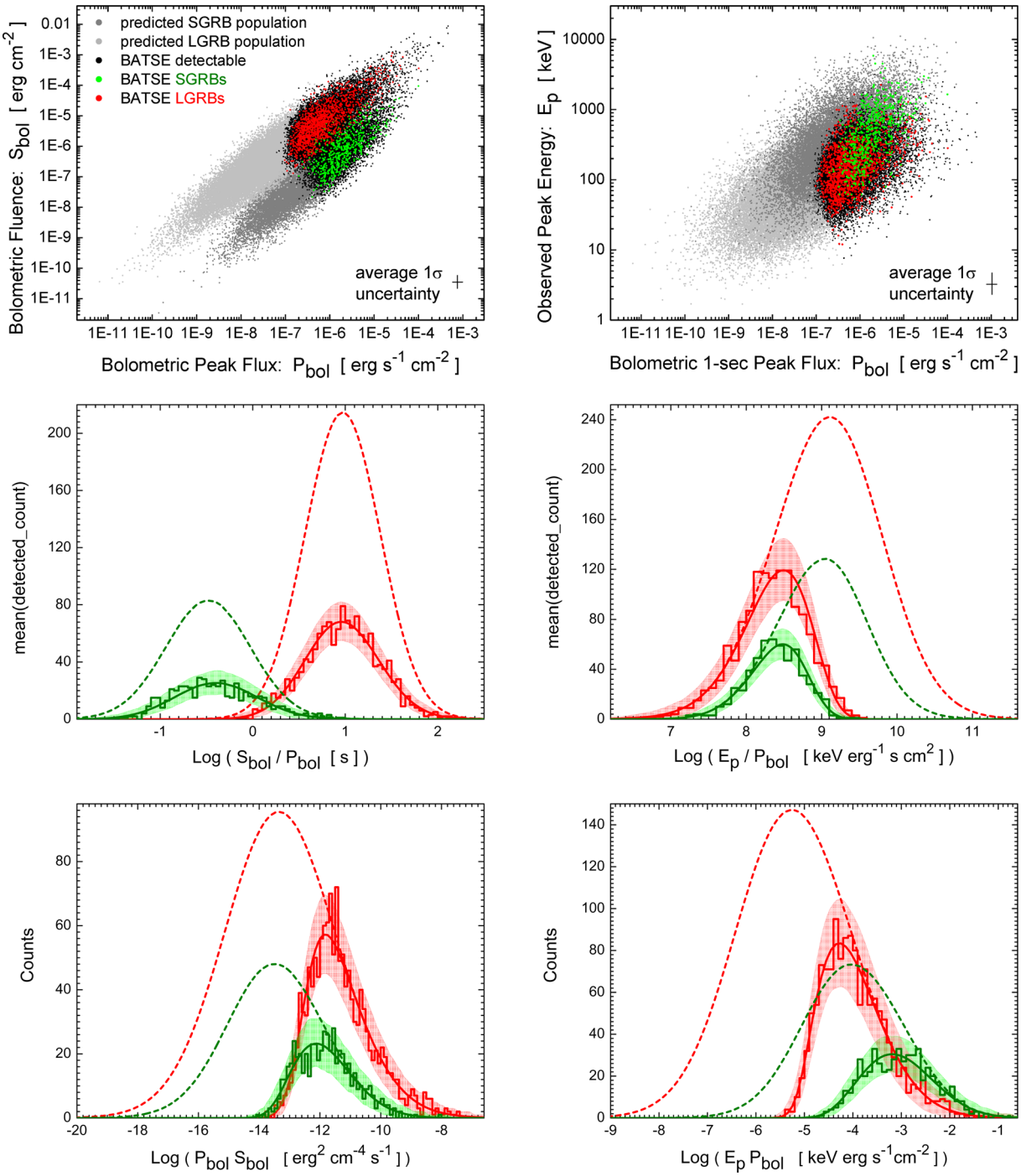

Figure 4. Bivariate predictions of the *multivariate* best-fitting SGRB and LGRB world models for BATSE catalogue GRBs, subject to BATSE detection threshold. Colours, line styles, and colour-shaded areas bear the same meaning as in Fig. 3. Evidence for potential systematic bias in peak flux measurements of BATSE GRBs close to detection threshold (Appendix B) can be seen in the centre-right and bottom-left plots of the figure. Fitting results for LGRBs are taken from Shahmoradi (2013b).

For the distribution of the intrinsic spectral peak energies of SGRBs, the model predicts an approximate 3σ range of $E_{\mathrm{p},z} \in [45\,\mathrm{keV}, 16\,\mathrm{MeV}]$, with an intrinsic average peak energy of $E_{\mathrm{p},z} \sim 955\,\mathrm{keV}$. This corresponds to an observer-frame 3σ range of $E_{\mathrm{p},z} \in [10\,\mathrm{keV}, 6\,\mathrm{MeV}]$, with an observer-frame average peak energy of $E_{\mathrm{p},z} \sim 300\,\mathrm{keV}$. For comparison, Shahmoradi (2013b) finds approximate 3σ ranges of $E_{\mathrm{p},z}(\mathrm{keV}) \in [20, 4000]$ and $E_{\mathrm{p}}(\mathrm{keV}) \in [5, 1430]$ for the intrinsic and observer-frame spectral peak energy distributions of LGRBs, with population averages $E_{\mathrm{p},z} \sim 300\,\mathrm{keV}$ & $E_{\mathrm{p}} \sim 85\,\mathrm{keV}$, respectively.

In contrast, the distributions of the observed spectral peak energies of *BATSE catalogue LGRBs and SGRBs* as found by Shahmoradi & Nemiroff (2010, fig. 13 therein) are $E_{\mathrm{p}} \sim 140(\mathrm{keV})$ and $E_{\mathrm{p}} \sim 520(\mathrm{keV})$, respectively, slightly larger than the inferred values for the underlying population of the two classes here in this work. Similarly, Nava et al. (2011) also find slightly larger average E_{p}

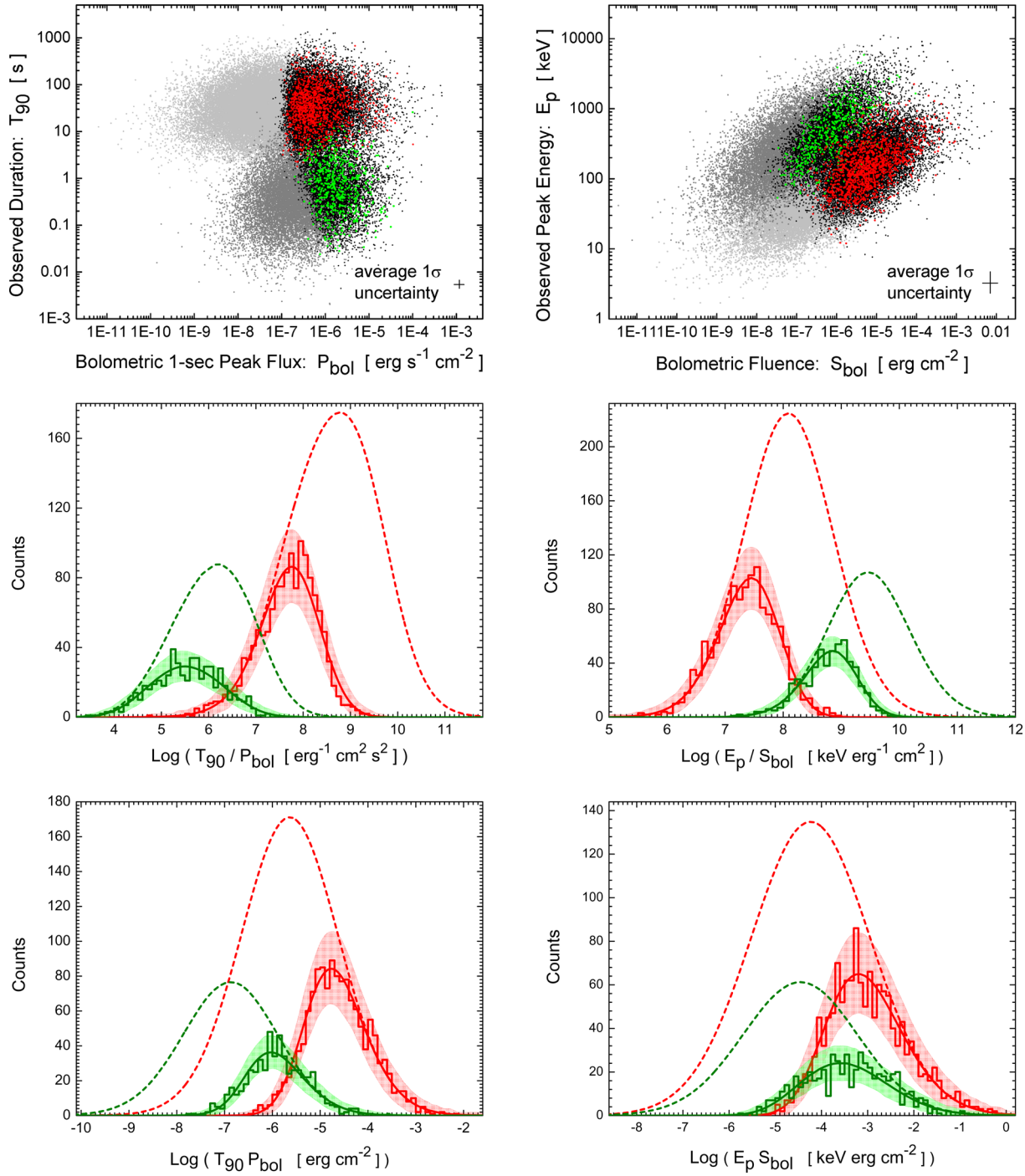

Figure 5. Bivariate predictions of the *multivariate* best-fitting SGRB and LGRB world models for BATSE catalogue GRBs, subject to BATSE detection threshold. Colours, line styles, and colour-shaded areas bear the same meaning as in Fig. 3. The apparent lack-of-fit in the top-left and centre-left plots indicates the potential systematic bias in the duration (T_{90}) measurements of the longest duration BATSE GRBs close to detection threshold (cf. Appendix B). Fitting results for LGRBs are taken from Shahmoradi (2013b).

values for a sample of 438 *Fermi* SGRBs and LGRBs. The discrepancy between the detected sample and the underlying population can be explained by sample incompleteness due to BATSE LAD and *Fermi*'s Gamma-ray Burst Monitor (GBM) detection thresholds. This is in line with previous findings on the role of selection effects due to gamma-ray detectors in shaping the observed properties of the two GRB classes (e.g. Band & Preece 2005; Butler et al. 2009; Shahmoradi & Nemiroff 2009, 2011; Kocevski 2012b).

As for the prompt duration of SGRBs, the model predicts a 3σ range of $T_{90,z} \in [2\,\mathrm{ms}, 7\,\mathrm{s}]$ for the intrinsic duration distribution of SGRBs with a population average of $T_{90,z} \sim 180\,\mathrm{ms}$. This corresponds to a 3σ dynamic range of $T_{90} \in [5\,\mathrm{ms}, 22\,\mathrm{s}]$ for the duration distribution of SGRBs in the observer frame with a population average of $T_{90} \sim 350\,\mathrm{ms}$. When compared to BATSE-detected sample of SGRBs with an average $T_{90} \sim 670\,\mathrm{ms}$, it is apparent that the majority of undetected SGRBs were likely

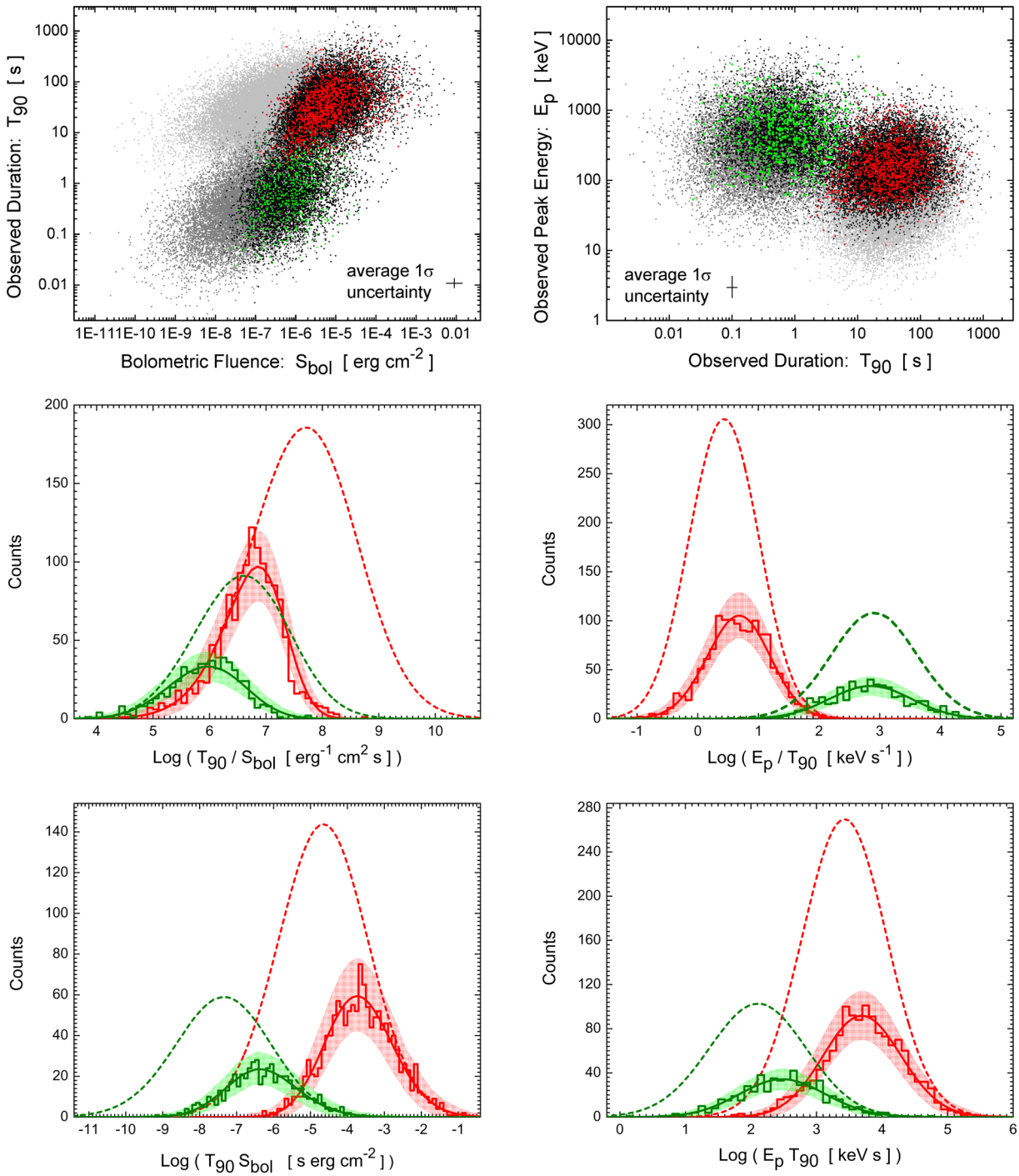

Figure 6. Bivariate predictions of the *multivariate* best-fitting SGRB and LGRB world models for BATSE catalogue GRBs, subject to BATSE detection threshold. Colours, line styles, and colour-shaded areas bear the same meaning as in Fig. 3. The apparent lack-of-fit in the top-left and centre-left plots indicates the potential systematic bias in the duration (T_{90}) measurements of the longest duration BATSE GRBs close to detection threshold (cf. Appendix B). Fitting results for LGRBs are taken from Shahmoradi (2013b).

among the shortest events in the population. This corroborates the early hints on the potential existence of very short-duration GRBs that could have been missed by BATSE LADs (e.g. figs 1 and 2 in Nemiroff et al. 1998). The minor excess predicted by the SGRB world model may also be partly attributed to the systematic biases and errors in BATSE data and the simplified model of BATSE trigger threshold for SGRBs as explained in Appendix A and B.

For comparison, the LGRB world model of Shahmoradi (2013b) predicts an approximate 3σ range of $T_{90,z}(s) \in [0.5, 145]$ for the intrinsic duration distribution of LGRBs with a population average of $T_{90,z} \sim 10s$, corresponding to an approximate 3σ dynamic range of $T_{90}(s) \in [1, 620]$ in the observer frame with a population average of $T_{90} \sim 30s$.

The presented LGRB and SGRB world models also predict that intrinsically shorter duration GRBs in both classes, although likely

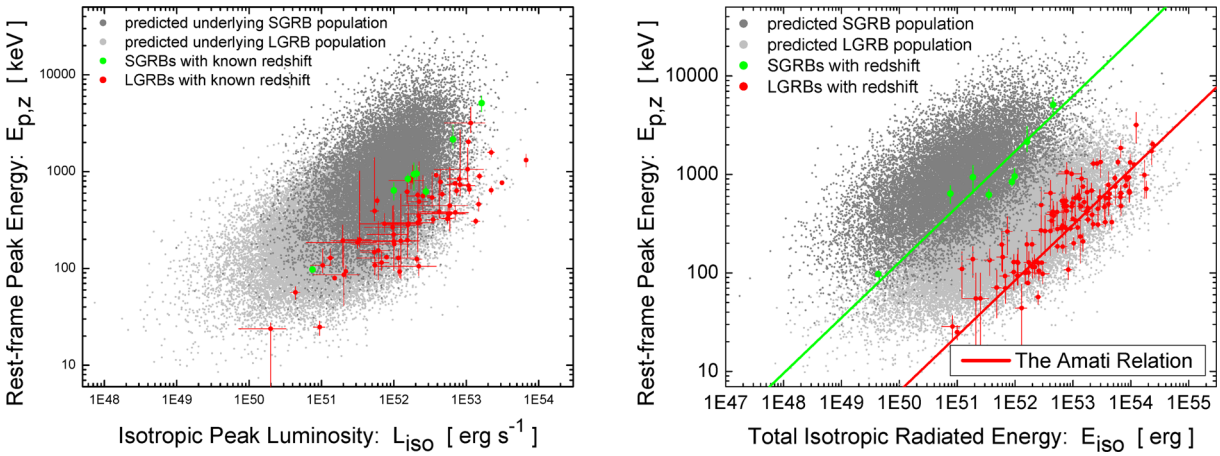

Figure 7. Prediction of the world model for the joint bivariate distributions of SGRBs in the rest-frame planes of L_{iso}–$E_{p,z}$ and E_{iso}–$E_{p,z}$. For comparison, the prediction of the world model for LGRBs population – the Amati & Yonetoku relations – are also shown (cf. Shahmoradi 2013b). The green filled circles represent SGRB data with known redshift (Zhang et al. 2012b; Tsutsui et al. 2013) and the red filled circles represent LGRB data taken from Schaefer (2007), Amati et al. (2008), and Ghirlanda et al. (2008).

exist, have lower chances of detection by gamma-ray instruments such as BATSE LAD and *Fermi* GBM. These results corroborate the recent findings of Littlejohns et al. (2013) and Littlejohns & Butler (2014) based on a sample of *Swift* LGRBs and further extend it to the population of SGRBs as illustrated in *right-hand plot* of Fig. 2.

4.3 Temporal and spectral correlations

There is already an extensive body of literature on the potential existence of correlations among the prompt spectral and temporal parameters of LGRBs (cf. Shahmoradi & Nemiroff 2011, for a comprehensive review of the literature). Much of the efforts so far has mainly focused on brightness–hardness types of relations, such as the Amati relation (E_{iso}–$E_{p,z}$) and the Yonetoku relation (L_{iso}–$E_{p,z}$). Currently, the general consensus is that these relations do exist with high significance (e.g. Butler et al. 2010; Shahmoradi 2013b), but with far less strength than the original findings of Amati et al. (2002) and Yonetoku et al. (2004). In addition to early hints on the potential existence of duration–brightness relations (e.g. Horvath et al. 2005), recently Butler et al. (2010) also found, through an elaborate and comprehensive analysis of *Swift* data, some tentative signatures of a significant positive correlation between the intrinsic duration and the total isotropic emission of LGRBs. Later, Shahmoradi (2013b) provided evidence in support of intrinsic duration–brightness correlations among LGRBs using independent methods and models applied to BATSE catalogue data, and further showed that the brightness–duration relations (i.e. E_{iso}–$T_{90,z}$ and L_{iso}–$T_{90,z}$) are of comparable strength and significance to brightness–hardness relations (i.e. E_{iso}–$E_{p,z}$ and L_{iso}–$E_{p,z}$). This positive correlation is also evident in the results of the LGRB world model in Table 2. Unlike the work of Shahmoradi (2013b), here in this work we have applied an energy band correction of the form $(1+z)^{-0.34}$ to the observed durations (T_{90}) of BATSE LGRBs (e.g. Gehrels et al. 2006; Butler et al. 2010). This correction if applied, slightly relaxes the strength of the correlation between the intrinsic duration and brightness.

Contrary to LGRBs, correlations among the prompt-emission parameters of SGRBs have been far less investigated. Recently, Zhang et al. (2012b) and Tsutsui et al. (2013) used a small sample of SGRBs with measured redshift to argue for the potential existence of intrinsic hardness–brightness correlations in the population of SGRBs similar to the class of LGRBs. Nevertheless, the strength and significance of these positive correlations in the underlying population of SGRBs could not be determined in their studies due to strong selection bias and sample incompleteness in observational data.

The results of the SGRB world model, as presented in Table 2, confirm the existence of intrinsic hardness–brightness correlations among SGRBs. Specifically, the model predicts highly significant correlation strengths of $\rho \sim 0.51 \pm 0.10$ & $\rho \sim 0.60 \pm 0.06$ for L_{iso}–$E_{p,z}$ and E_{iso}–$E_{p,z}$ relations, respectively. The two correlation strengths are very similar to the predictions of the LGRB world model for the same relations in the population of LGRBs ($\rho \sim 0.45 \pm 0.07$ and $\rho \sim 0.58 \pm 0.04$, respectively). This is illustrated in the plots of Fig. 7.

The similarity of the two GRB classes in the joint distributions and correlations is not limited to only hardness–brightness relations. Indeed, all four prompt-emission variables in both populations (L_{iso}, E_{iso}, $E_{p,z}$, $T_{90,z}$) appear to be similarly related to each other in both populations, as shown in Table 2.

A potential correlation of the form

$$E_{p,z}\sqrt{T_{90,z}} \propto E_{\gamma} \tag{12}$$

has also been derived and suggested by Putten (2008), in which E_{γ} stands for the beaming-angle-corrected output energy from the burst. The presented analysis is consistent with the existence of such universal relation. The strength and significance of it however, cannot be determined solely based on BATSE observational data, as it requires a knowledge of redshift and the beaming angle of individual events. We also caution against the use of the hardness–brightness correlations, such as the Amati relation, to infer the characteristics of the inner engines of the two GRB classes. Our predictions based on BATSE catalogue GRBs is that the Amati relation in its current form – as presented by Putten et al. (2014) – is likely strongly affected by sample incompleteness. In addition, the significant overlap of the two GRB populations in hardness–brightness plots, as illustrated in Fig. 7, likely renders the Amati relation an ineffective tool for GRB classification.

5 CONCLUDING REMARKS

The primary goal of the presented analysis was to constrain the energetics, luminosity function, and the prompt gamma-ray correlations of short-hard class of GRBs, using the wealth of information that has remained untouched in the largest catalogue of GRBs available to this date, the current BATSE GRB catalogue. In the following lines we summarize the steps we have taken to constrain the population properties of short-hard and similarly, long-soft GRBs (SGRBs and LGRBs, respectively):

(i) A sample of 565 short-hard and 1366 long-soft bursts were first segregated and selected from the current BATSE catalogue of 2130 GRBs, for which complete data were available, including the bolometric peak flux ($P_{\rm bol}$), the bolometric fluence ($S_{\rm bol}$), the observed spectral peak energy ($E_{\rm p}$), and the observed duration (T_{90}). The classification method is based on fuzzy clustering algorithms on the two prompt-emission variables $E_{\rm p}$ and T_{90} which are least affected by the detection threshold of gamma-ray detectors (Section 2.1). This methodology can be readily applied to other GRB catalogues, in particular *Fermi* GBM.

(ii) We propose that the intrinsic joint distribution of the four main prompt-emission parameters of SGRBs – the isotropic peak gamma-ray luminosity ($L_{\rm iso}$), the total isotropic gamma-ray emission ($E_{\rm iso}$), the intrinsic spectral peak energy ($E_{\rm p,z}$), and the intrinsic duration ($T_{90,z}$) – can be well described as a multivariate (four-dimensional) lognormal distribution, once the observational data is corrected for effects of detection threshold and sample incompleteness (Section 2.2).

(iii) The best-fitting parameters of the model are then found by maximizing the likelihood function of the model given BATSE SGRB data (equation 9) subject to the Bayesian priors of equation (11), with an SGRB rate density (equation 7) that is the result of the convolution of SFR (equation 5) with a lognormal binary merger delay distribution of equation (6). The resulting best-fitting parameters are summarized in Table 2.

We highlight, in the following lines, the main conclusions of the presented analysis and the important similarities and differences that we find in the prompt gamma-ray emission properties of the two classes of short-hard and long-soft GRBs.

(i) **Population distribution**

The population distributions of LGRBs and SGRBs appears to be well described by two separate multivariate lognormal distributions in the four-dimensional parameter space of the isotropic peak gamma-ray luminosity ($L_{\rm iso}$), total isotropic gamma-ray emission ($E_{\rm iso}$), the intrinsic spectral peak energy ($E_{\rm p,z}$), and the intrinsic duration ($T_{90,z}$), once corrected for the effects of detector threshold and sample incompleteness. This is in line with previous findings of Shahmoradi (2013b) and Shahmoradi (2013a).

(ii) **GRB classification**

According to the predictions of our GRB world, the most accurate and the quickest method of individual GRB classification – solely based on prompt emission properties – appears to be the observer-frame ratio $E_{\rm p}/T_{90}[{\rm keV\,s^{-1}}]$. We find that 99 per cent of all LGRBs have $E_{\rm p}/T_{90} \lesssim 50$, and 95 per cent of all SGRBs have $E_{\rm p}/T_{90} \gtrsim 50$ (cf. Fig. 6, *centre right*).

We caution against the use of other similar quantities, such as the ratio of the observed spectral peak energy to bolometric fluence $E_{\rm p}/S_{\rm bol}$ as proposed by Goldstein et al. (2010). Although this ratio seems to be a good discriminator in the sample of *detected* GRBs, it is strongly affected by sample incompleteness and detector threshold effects. Fig. 5 (*centre right*) illustrates the effects of sample incompleteness on the observed distribution of this ratio.

(iii) **Energetics and luminosity function**

The presented GRB world model predicts a 3σ range of $L_{\rm iso}({\rm erg\,s^{-1}}) \in [10^{50}, 10^{53}]$ for the 64-ms isotropic peak luminosity of SGRBs. A translation of this range to 1024-ms peak luminosity using equation (A3) approximately corresponds to $L_{\rm iso}({\rm erg\,s^{-1}}) \in [8 \times 10^{48}, 1.3 \times 10^{53}]$. This range is very close and similar to the predictions of the GRB world model for 1024-ms peak luminosity distribution of LGRBs with a 3σ range of $L_{\rm iso}({\rm erg\,s^{-1}}) \in [3.2 \times 10^{49}, 3.2 \times 10^{53}]$.

Also predicted by the model are the 3σ ranges of $E_{\rm iso}({\rm erg}) \in [10^{48}, 3.2 \times 10^{53}]$ and $E_{\rm iso}({\rm erg}) \in [1.6 \times 10^{49}, 5.0 \times 10^{54}]$ for the total isotropic gamma-ray emission of SGRBs and LGRBs, respectively. The two variables $L_{\rm iso}$ and $E_{\rm iso}$ are strongly correlated with each other in both GRB classes (cf. Table 2).

(iv) **Prompt duration and spectral peak energy**

The population distribution of the *rest-frame* spectral peak energies ($E_{\rm p,z}$) of both SGRBs and LGRBs appears to be described well by lognormal distributions with population averages $E_{\rm p,z} \sim 955\,{\rm keV}$ and $E_{\rm p,z} \sim 300\,{\rm keV}$, and 3σ ranges $E_{\rm p,z} \in [45\,{\rm keV}, 16\,{\rm MeV}]$ and $E_{\rm p,z} \in [10\,{\rm keV}, 6\,{\rm MeV}]$, respectively. In the observer frame, this corresponds approximately to average $E_{\rm p,\,z} \sim 300\,{\rm keV}$ and $E_{\rm p,z} \sim 85\,{\rm keV}$ with 3σ ranges $E_{\rm p}({\rm keV}) \in [20, 4000]$ and $E_{\rm p}({\rm keV}) \in [5, 1430]$ for the two SGRB and LGRB classes, respectively.

While the underlying duration distribution of LGRBs ($T_{90,z}$) does not seem to be significantly affected by the detection threshold of BATSE LADs, there is tentative evidence that very short-duration SGRBs had, in general, lower chances of detection by BATSE (Fig. 3, *bottom right*). For the population of SGRBs, we find a 3σ range of intrinsic duration $T_{90,z}(s) \in [0.002, 7]$ with a population average of $T_{90,z} \sim 180\,{\rm ms}$. In contrast, for $T_{90,z}$ distribution of LGRBs we find a 3σ range of $T_{90,z}(s) \in [0.5, 145]$ with population average $T_{90,z} \sim 10s$ (Section 4.2).

(v) **Prompt gamma-ray correlations**

All four prompt gamma-ray variables appear to be strongly and positively correlated with each other in both GRB classes, with the exception of the two variables $E_{\rm p,z}$ and $T_{90,z}$ which tend to be weakly, yet positively, correlated with each other. The intrinsic *hardness–brightness* relations (e.g. the Amati & the Yonetoku relations) are confirmed but with much higher dispersions than originally reported for these relations (Fig. 7). The presented GRB world model reveals startling similarities in the strengths of the corresponding hardness–brightness correlations in the two GRB classes. Specifically, the model predicts a Pearson's correlation strength of $\rho \sim 0.6$ for $E_{\rm iso}$–$E_{\rm p,z}$ relation and $\rho \sim 0.5$ for $L_{\rm iso}$–$E_{\rm p,z}$ relation, similarly in both GRB classes.

The presented GRB model also predicts intrinsic *duration–brightness* correlations that are almost identical in strength between the two GRB classes, also very similar to the correlation strengths of hardness–brightness relations (cf. Table 2 and Section 4.3).

In summary, we have presented a mathematical model with minimal free parameters that enables us, for the first time, to constrain the main characteristics of the prompt gamma-ray emission of short-hard and long-soft GRBs, jointly and simultaneously, while paying careful attention to selection biases and sample incompleteness due to gamma-ray detector thresholds. Our model predicts a high level of similarity in the joint population distribution of the prompt-emission properties of the two GRB classes, a finding that merits further investigation of the potential similarities in the prompt emission mechanisms of both GRB classes .

REFERENCES

Amati L. et al., 2002, A&A, 390, 81
Amati L., Guidorzi C., Frontera F., Della Valle M., Finelli F., Landi R., Montanari E., 2008, MNRAS, 391, 577
Backus J., 1978, ACM SIGPLAN Not., 13, 165
Balastegui A., Ruiz-Lapuente P., Canal R., 2001, MNRAS, 328, 283
Balazs L. G., Bagoly Z., Horvath I., Mszros A., Mszros P., 2003, A&A, 401, 129
Band D. L., 2003, ApJ, 588, 945
Band D. L., 2006, ApJ, 644, 378
Band D. L., Preece R. D., 2005, ApJ, 627, 319
Band D. et al., 1993, ApJ, 413, 281
Band D. L. et al., 2008, ApJ, 673, 1225
Belczynski K., Perna R., Bulik T., Kalogera V., Ivanova N., Lamb D. Q., 2006, ApJ, 648, 1110
Belczynski K., Holz D. E., Fryer C. L., Berger E., Hartmann D. H., O'Shea B., 2010, ApJ, 708, 117
Berger E., 2011, New Astron. Rev., 55, 1
Berger E., 2014, ARA&A, 52, 43
Berger E. et al., 2007, ApJ, 664, 1000
Bezdek J. C., 1981, Pattern Recognition with Fuzzy Objective Function Algorithms. Kluwer, Norwell, MA
Bogomazov A. I., Lipunov V. M., Tutukov A. V., 2007, Astron. Rep., 51, 308
Browne W. J., 2006, Comput. Stat. Data Anal., 50, 1655
Butler N. R., Kocevski D., Bloom J. S., Curtis J. L., 2007, ApJ, 671, 656
Butler N. R., Kocevski D., Bloom J. S., 2009, ApJ, 694, 76
Butler N. R., Bloom J. S., Poznanski D., 2010, ApJ, 711, 495
Calderone G. et al., 2015, MNRAS, 448, 403
Campisi M. A., Li L.-X., Jakobsson P., 2010, MNRAS, 407, 1972
Chapman R., Priddey R. S., Tanvir N. R., 2009, MNRAS, 395, 1515
Chattopadhyay T., Misra R., Chattopadhyay A. K., Naskar M., 2007, ApJ, 667, 1017
Coward D. M. et al., 2012, MNRAS, 425, 2668
Coward D., Howell E., Branchesi M., Gendre B., Stratta G., 2013, preprint (arXiv:1305.3366)
Czerny B., Janiuk A., Cline D. B., Otwinowski S., 2011, New Astron., 16, 33
D'Avanzo P. et al., 2014, MNRAS, 442, 2342
Dainotti M. G., Ostrowski M., Willingale R., 2011, MNRAS, 418, 2202
Dainotti M. G., Cardone V. F., Piedipalumbo E., Capozziello S., 2013, MNRAS, 436, 82
Dainotti M. G., Del Vecchio R., Shigehiro N., Capozziello S., 2015, ApJ, 800, 31
Dezalay J.-P., Barat C., Talon R., Syunyaev R., Terekhov O., Kuznetsov A., 1992, in Paciesas W., Fishman G. J., eds, AIP Conf. Proc. Vol. 265, Gamma-ray Bursts. Am. Inst. Phys., New York, p. 304
Dunn J. C., 1973, J. Cybern., 3, 32
Eichler D., Livio M., Piran T., Schramm D. N., 1989, Nature, 340, 126
Fenimore E. E., in 't Zand J. J. M., Norris J. P., Bonnell J. T., Nemiroff R. J., 1995, ApJ, 448, L101
Fisher R., 1915, Biometrika, 10, 507
Gao H., Lu Y., Zhang S. N., 2010, ApJ, 717, 268
Gehrels N. et al., 2004, ApJ, 611, 1005
Gehrels N. et al., 2006, Nature, 444, 1044
Gehrels N., Ramirez-Ruiz E., Fox D. B., 2009, ARA&A, 47, 567
Ghirlanda G., Nava L., Ghisellini G., Firmani C., Cabrera J. I., 2008, MNRAS, 387, 319
Ghirlanda G., Ghisellini G., Nava L., Burlon D., 2011, MNRAS, 410, L47
Goldstein A., Preece R. D., Briggs M. S., 2010, ApJ, 721, 1329
Goldstein A., Preece R. D., Mallozzi R. S., Briggs M. S., Fishman G. J., Kouveliotou C., Paciesas W. S., Burgess J. M., 2013, ApJS, 208, 21
Guelbenzu A. N. et al., 2014, ApJ, 789, 45
Guetta D., Piran T., 2006, A&A, 453, 823
Guetta D., Piran T., Waxman E., 2005, ApJ, 619, 412
Haario H., Saksman E., Tamminen J., 2001, Bernoulli, 7, 223
Hakkila J., Haglin D. J., Roiger R. J., Mallozzi R. S., Pendleton G. N., Meegan C. A., 2000a, in Kippen R. M., Mallozzi R. S., Fishman G. J., eds, AIP Conf. Proc. Vol. 526, Gamma-ray Bursts: 5th Huntsville Symposium. Am. Inst. Phys., New York, p. 33
Hakkila J., Meegan C. A., Pendleton G. N., Mallozzi R. S., Haglin D. J., Roiger R. J., 2000b, in Kippen R. M., Mallozzi R. S., Fishman G. J., eds, AIP Conf. Proc. Vol. 526, Gamma-ray Bursts: 5th Huntsville Symposium. Am. Inst. Phys., New York, p. 48
Hakkila J., Haglin D. J., Pendleton G. N., Mallozzi R. S., Meegan C. A., Roiger R. J., 2000c, ApJ, 538, 165
Hakkila J., Mallozzi R. S., Roiger R. J., Haglin D. J., Pendleton G. N., Meegan C. A., 2001, in Costa E., Frontera F., Hjorth J., eds, Tools for Gamma-Ray Burst Data Mining. Springer, Berlin Heidelberg, p. 60
Hakkila J., Giblin T. W., Roiger R. J., Haglin D. J., Paciesas W. S., Meegan C. A., 2003a, ApJ, 582, 320
Hakkila J., Pendleton G. N., Meegan C. A., Briggs M. S., Kippen R. M., Preece R. D., 2003b, in Ricker G. R., Vanderspek R. K., eds, AIP Conf. Proc. Vol. 662, Gamma-ray Burst and Afterglow Astronomy 2001: A Workshop Celebrating the First Year of the HETE Mission. Am. Inst. Phys., New York, p. 176
Hakkila J., Giblin T. W., Roiger R. J., Haglin D. J., Pačiesas W. S., Meegan C. A., 2004, Balt. Astron., 13, 211
Hao J.-M., Yuan Y.-F., 2013, A&A, 558, 22
Hobson M. P., Jaffe A. H., Liddle A. R., Mukeherjee P., Parkinson D., 2010, Bayesian Methods in Cosmology. Cambridge Univ. Press, Cambridge
Hogg D. W., Turner E. L., 1998, PASP, 110, 727
Hopkins A. M., Beacom J. F., 2006, ApJ, 651, 142
Hopman C., Guetta D., Waxman E., Portegies Zwart S., 2006, ApJ, 643, L91
Horvath I., 1998, ApJ, 508, 757
Horvath I., Balazs L. G., Meszaros P., Bagoly Z., Meszaros A., 2005, preprint (astro-ph/0508023)
Horvath I., Balzs L. G., Bagoly Z., Ryde F., Mszros A., 2006, A&A, 447, 23
Horvath I., Balzs L. G., Bagoly Z., Veres P., 2008, A&A, 489, L1
Horvath I., Balzs L. G., Hakkila J., Bagoly Z., Preece R. D., 2012, p. 46
Howell E. J., Coward D. M., Stratta G., Gendre B., Zhou H., 2014, MNRAS, 444, 15
Jarosik N. et al., 2011, ApJS, 192, 14
John Barnard R. M., 2000, Stat. Sin., 10, 1281
Kóbori J., Bagoly Z., Balzs L. G., Horvath I., 2014, preprint (arXiv:1407.2760)
Kocevski D., 2012a, in Rau A., Greiner J., eds, Proceedings of the Gamma-Ray Bursts 2012 Conference (GRB 2012), 17, Available at: http://pos.sissa.it/cgi-bin/reader/conf.cgi?confid=152
Kocevski D., 2012b, ApJ, 747, 146
Koshut T. M., Paciesas W. S., Kouveliotou C., van Paradijs J., Pendleton G. N., Fishman G. J., Meegan C. A., 1996, ApJ, 463, 570
Kouveliotou C., Meegan C. A., Fishman G. J., Bhat N. P., Briggs M. S., Koshut T. M., Paciesas W. S., Pendleton G. N., 1993, ApJ, 413, L101
Levan A. J. et al., 2014, ApJ, 781, 13
Li L.-X., 2008, MNRAS, 388, 1487
Lien A., Sakamoto T., Gehrels N., Palmer D. M., Barthelmy S. D., Graziani C., Cannizzo J. K., 2013, preprint (arXiv:1308.3720)
Lien A., Sakamoto T., Gehrels N., Palmer D. M., Barthelmy S. D., Graziani C., Cannizzo J. K., 2014, ApJ, 783, 24
Littlejohns O. M., Butler N. R., 2014, MNRAS, 444, 3948
Littlejohns O. M., Tanvir N. R., Willingale R., Evans P. A., O'Brien P. T., Levan A. J., 2013, MNRAS, 436, 3640
Loredo T. J., 2004, in Fischer R., Preuss R., von Toussaint U., eds, AIP Conf. Proc. Vol. 735, Bayesian Inference and Maximum Entropy Methods in Science and Engineering. Am. Inst. Phys., New York, p. 195
Lü H.-J., Liang E.-W., Zhang B.-B., Zhang B., 2010, ApJ, 725, 1965
Lü H.-J., Zhang B., Liang E.-W., Zhang B.-B., Sakamoto T., 2014, MNRAS, 442, 1922
Mazets E. P. et al., 1981, Ap&SS, 80, 3
Meegan C. A., Fishman G. J., Wilson R. B., Horack J. M., Brock M. N., Paciesas W. S., Pendleton G. N., Kouveliotou C., 1992, Nature, 355, 143

Metcalf M., Reid J., Cohen M., 2011, Modern Fortran Explained. Oxford Univ. Press, Oxford
Michelson P. F., Atwood W. B., Ritz S., 2010, Rep. Prog. Phys., 73, 074901
Mukherjee S., Feigelson E. D., Babu G. J., Murtagh F., Fraley C., Raftery A., 1998, ApJ, 508, 314
Nakar E., 2007, Phys. Rep., 442, 166
Nakar E., Piran T., 2005, MNRAS, 360, L73
Nakar E., Gal-Yam A., Fox D. B., 2006, ApJ, 650, 281
Narayan R., Paczynski B., Piran T., 1992, ApJ, 395, L83
Nava L., Ghirlanda G., Ghisellini G., Firmani C., 2008, MNRAS, 391, 639
Nava L., Ghirlanda G., Ghisellini G., Celotti A., 2011, A&A, 530, 21
Nemiroff R. J., 2000, ApJ, 544, 805
Nemiroff R. J., Norris J. P., Bonnell J. T., Wickramasinghe W. A. D. T., Kouveliotou C., Paciesas W. S., Fishman G. J., Meegan C. A., 1994, ApJ, 435, L133
Nemiroff R. J., Norris J. P., Bonnell J. T., Marani G. F., 1998, ApJ, 494, L173
Norris J. P., Cline T. L., Desai U. D., Teegarden B. J., 1984, Nature, 308, 434
O'Shaughnessy R., Belczynski K., Kalogera V., 2008, ApJ, 675, 566
Paciesas W. S. et al., 1999, ApJS, 122, 465
Paczynski B., 1986, ApJ, 308, L43
Pescalli A., Ghirlanda G., Salafia O. S., Ghisellini G., Nappo F., Salvaterra R., 2015, MNRAS, 447, 1911
Putten M. H. P. M. v., 2008, ApJ, 685, L63
Putten M. H. P. M. v., Lee G. M., Valle M. D., Amati L., Levinson A., 2014, MNRAS, 444, L58
Qin Y.-P., Chen Z.-F., 2013, MNRAS, 430, 163
Qin Y. et al., 2013, ApJ, 763, 15
Salvaterra R., Cerutti A., Chincarini G., Colpi M., Guidorzi C., Romano P., 2008, MNRAS, 388, L6
Schaefer B. E., 2007, ApJ, 660, 16
Shahmoradi A., 2013a, preprint (arXiv:1308.1097)
Shahmoradi A., 2013b, ApJ, 766, 111
Shahmoradi A., Nemiroff R., 2009, in Meegan C., Kouveliotou C., Gehrels N., eds, AIP Conf. Proc. Vol. 1133, Gamma-ray Burst: Sixth Huntsville Symposium. Am. Inst. Phys., New York, p. 425
Shahmoradi A., Nemiroff R. J., 2010, MNRAS, 407, 2075
Shahmoradi A., Nemiroff R. J., 2011, MNRAS, 411, 1843
Stern B. E., Tikhomirova Y., Kompaneets D., Svensson R., Poutanen J., 2001, ApJ, 563, 80
Stern B. E., Atteia J.-L., Hurley K., 2002, ApJ, 578, 304
Tsutsui R., Yonetoku D., Nakamura T., Takahashi K., Morihara Y., 2013, MNRAS, 431, 1398
Virgili F. J., Liang E.-W., Zhang B., 2009, MNRAS, 392, 91
Virgili F. J., Zhang B., O'Brien P., Troja E., 2011, ApJ, 727, 109
Wanderman D., Piran T., 2010, MNRAS, 406, 1944
Wanderman D., Piran T., 2015, MNRAS, 448, 3026
Wickramasinghe T., Ukwatta T. N., 2010, MNRAS, 406, 548
Yonetoku D., Murakami T., Nakamura T., Yamazaki R., Inoue A. K., Ioka K., 2004, ApJ, 609, 935
Zhang B. et al., 2009, ApJ, 703, 1696
Zhang F.-W., Shao L., Yan J.-Z., Wei D.-M., 2012a, ApJ, 750, 88
Zhang Z. B., Chen D. Y., Huang Y. F., 2012b, ApJ, 755, 55
Zhang B.-B., Zhang B., Murase K., Connaughton V., Briggs M. S., 2014, ApJ, 787, 66
Zheng Z., Ramirez-Ruiz E., 2007, ApJ, 665, 1220

APPENDIX A: BATSE DETECTION THRESHOLD

An accurate modelling of the detection threshold of gamma-ray instruments is an integral part of any population study of GRBs. We have already argued in Section 2.2 that modelling the trigger efficiency of gamma-ray detectors solely based on a measure of peak photon/energy flux – as is generally done in most GRB population studies – can potentially lead to systematic biases in the derived quantities. Although, the detection efficiency of most gamma-ray detectors depends solely on the observed peak *photon* flux in a limited energy window, the quantity of interest that is most often modelled and studied is the *bolometric* peak flux ($P_{\rm bol}$). This variable depends on the observed peak photon flux and the spectral peak energy ($E_{\rm p}$) for the class of LGRBs (e.g. Shahmoradi 2013b), also on the observed duration (e.g. T_{90}) of the burst for the class of SGRBs. The effect of GRB duration on the peak flux measurement is very well illustrated in the *left-hand* plot of Fig. A1, where we show that for GRBs with $T_{90} \lesssim 1024$ ms, the time-scale used for the definition of the peak flux does indeed matter. This is particularly important in modelling the triggering algorithm of BATSE LADs, when a short burst could be potentially detected on any of the three different peak flux time-scales used in the triggering algorithm: 64, 256, and 1024 ms. Therefore, we adopt the following approach to construct a minimally biased model of BATSE trigger efficiency for the population study of short-hard bursts.

First, since only one definition (i.e. time-scale) of the bolometric peak flux can be incorporated in the SGRB world model of Section 2.2, we use the least-biased definition of peak flux for SGRBs – the 64-ms time-scale definition – in the GRB world model. Although, this definition is duration independent for virtually all BATSE GRBs, it becomes an increasingly biased measure of the peak flux for very long duration GRBs ($T_{90} \gg 1$ s) close to detection threshold. We then approximate the three *discrete* time-scale trigger efficiency of BATSE LADs with a sigmoidal function that increases monotonically with increasing duration of the burst, from 64 to 1024 ms. In other words, we convert the 64-ms peak flux used in our GRB world model to an effective *triggering* peak flux $P_{\rm eff}$ [erg s^{-1}], for which the detection efficiency of BATSE becomes duration-independent.

To expand on this, consider an idealized GRB light curve containing only a single square-shaped pulse with an exact duration of 64 ms and a signal strength that is four times the required significance for its detection on a 64-ms peak flux time-scale. In contrast, if there were only one triggering time-scale 1024 ms available on BATSE, the signal strength of this 64 ms event would fall right on the detection threshold of BATSE LADs. Thus, a 64 ms burst of peak flux P_{64} [ph s^{-1}] would be equivalent to an effective 1024 ms peak flux,

$$P_{\rm eff}\ [\mathrm{ph\ s^{-1}}] = \frac{1}{4} P_{64}\ [\mathrm{ph\ s^{-1}}], \tag{A1}$$

for the triggering algorithm of BATSE on a 1024-ms time-scale.

In reality however, GRB light curves are far more diverse than a single square pulse. Thus in order to build a more realistic model of BATSE LAD triggering algorithm, we fit a *complementary* error function of the mathematical form

$$\mathrm{erfc}(x) = \frac{2}{\sqrt{\pi}} \int_x^\infty \mathrm{e}^{-t^2} \mathrm{d}t, \tag{A2}$$

to the logarithm of the ratio of 64 to 1024 ms peak fluxes ($R_{\rm P_{64}/P_{1024}}$) as a function of the observed duration (T_{90}) of BATSE GRBs, as illustrated in the *left-hand plot* of Fig. A1. The resulting best-fitting function for $R_{\rm P_{64}/P_{1024}}$ has the form,

$$\log\left(R_{\rm P_{64}/P_{1024}}\right) \simeq 0.15 + 0.56 \times \mathrm{erfc}\left(\frac{\log(T_{90}) + 0.48}{1.05}\right). \tag{A3}$$

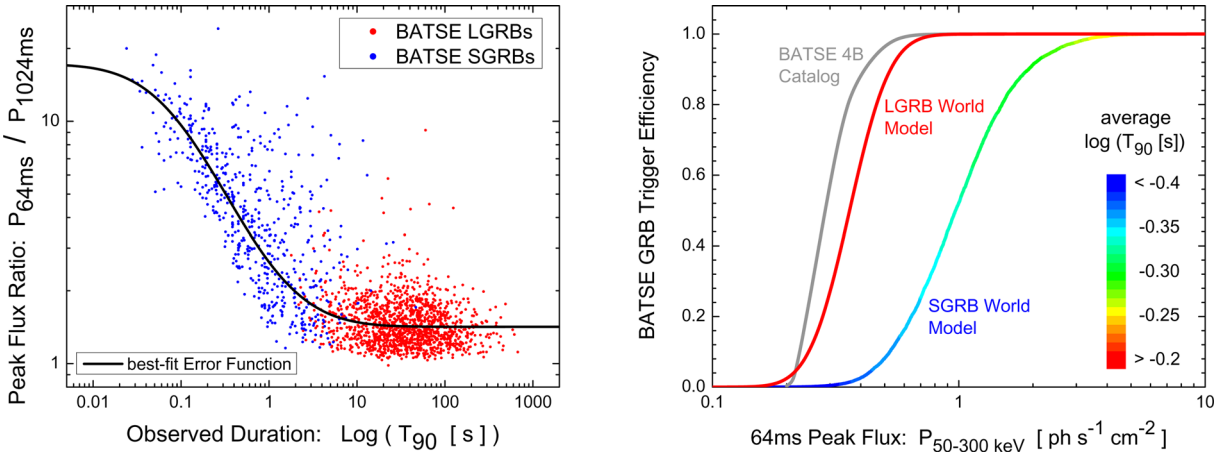

Figure A1. Left: an illustration of the higher detection probability of SGRBs on 64-ms time-scale peak flux towards very short durations compared to the commonly used 1024-ms peak flux definition for LGRBs. The duration dependence of the ratio of the two peak flux definitions highlights the inadequacy of the conventional definition of peak flux based on 1024-ms time binning for the detection of SGRBs. Right: the detection probabilities of BATSE GRBs according to the best-fitting SGRB and LGRB world models as a function of the peak 64-ms photon flux in BATSE detection energy range. For comparison, the nominal BATSE 4B catalogue trigger efficiency (Paciesas et al. 1999) for LGRBs is also shown by the grey solid line. It is evident from the efficiency curves that the very short SGRBs have on average lower detection probabilities compared to the longer duration events, while the detection probability of LGRBs is almost completely indifferent to the observed duration of the burst. This is also illustrated in the top-left plot of Fig. 5.

The effective *triggering* peak flux in the SGRB world model is then calculated using the following relation:

$$\log(P_{\rm eff}) \simeq \log(P_{64}) - \frac{1}{2}(\log(R_{\rm P_{64}/P_{1024}}) - 0.15). \quad \text{(A4)}$$

Once $P_{\rm eff}$ is obtained, we follow the approach of Shahmoradi (2013b) to calculate the detection probability (η) of a given SGRB with an effective *triggering* peak flux $P_{\rm eff}$,

$$\eta(\text{detection}|\mu_{\rm thresh}, \sigma_{\rm thresh}, L_{\rm iso}, E_{\rm p,z}, T_{90,z}, z) = \frac{1}{2} + \frac{1}{2}\,\text{erf}\left(\frac{\log(P_{\rm eff}(L_{\rm iso}, E_{\rm p,z}, T_{90,z}, z) - \mu_{\rm thresh})}{\sqrt{2}\sigma_{\rm thresh}}\right), \quad \text{(A5)}$$

where $\mu_{\rm thresh}$ and $\sigma_{\rm thresh}$ are the detection threshold parameters that are found by fitting the SGRB world model to BATSE observational data (cf. Table 2), and $P_{\rm eff}(L_{\rm iso}, E_{\rm p,z}, T_{90,z}, z)$ is the 1024-ms effective triggering peak flux in BATSE energy range of detection, 50–300[keV], calculated from the 64-ms peak flux ($P_{64}(L_{\rm iso}, E_{\rm p,z}, z)$ [ph s^{-1}]) in BATSE detection energy range using equation (A4). The connection between the rest-frame GRB parameters, $L_{\rm iso}$ and $E_{\rm p,z}$,z, and the 64-ms peak flux P_{64} is obtained by fitting a smoothly broken power law known as the Band model (Band et al. 1993) of the mathematical form

$$\Phi(E) \propto \begin{cases} E^{\alpha}\, e^{\left(-\frac{(1+z)(2+\alpha)E}{E_{\rm p,z}}\right)} & \text{if } E \le \left(\frac{E_{\rm p,z}}{1+z}\right)\left(\frac{\alpha-\beta}{2+\alpha}\right) \\ E^{\beta} & \text{if otherwise} \end{cases}, \quad \text{(A6)}$$

to SGRBs differential photon spectra, such that,

$$P_{64}(L_{\rm iso}, E_{\rm p,z}, z) = \frac{L_{\rm iso}}{4\pi {D_{\rm L}}^2(z)} \frac{\int_{50}^{300} \Phi\, dE}{\int_{\frac{0.1}{1+z}}^{\frac{20000}{1+z}} E\Phi\, dE}, \quad \text{(A7)}$$

where $D_{\rm L}(z)$ is the luminosity distance of equation (3). In order to bring the above calculations into the realm of current computational technologies, we simplify the integration limits in the denominator of equation (A7) to a redshift-independent energy range [0.1 keV, 20 MeV] and fix the low- and high-energy photon indices of the Band model (equation A6) to their corresponding population averages $\alpha = -1.1$ and $\beta = -2.3$. Butler et al. (2010) show that these simplifications result in an uncertainty of <0.05 dex in the estimated peak flux, which is negligible compared to the existing systematic biases in BATSE data (cf. Appendix B and uncertainties in the spectral peak energy estimates of Shahmoradi & Nemiroff 2010 used in this work). The resulting best-fitting model of BATSE detection efficiency as a function of P_{64} for the class of short-hard bursts is illustrated and compared to the detection efficiency of long-soft bursts in the *right-hand* plot of Fig. A1.

APPENDIX B: SYSTEMATIC BIASES IN BATSE GRB DATA

As argued by Hogg & Turner (1998), astronomical catalogues and surveys are prone to systematic biases in measurements, in particular, close to the detection threshold of the observational instruments. The BATSE catalogue of GRBs is no exception to such biases, also noted by BATSE team and others (e.g. Nemiroff et al. 1994; Paciesas et al. 1999; Stern et al. 2001; Stern, Atteia & Hurley 2002). Although, throughout this work we relied on BATSE catalogue data in their original form, here we present the results of our search for the potential signatures of systematic biases in BATSE data, which will pave the way for more accurate and rigorous population studies of GRBs in future.

In order to identify the extent of systematic bias in BATSE GRB data close to detection threshold, we first calculate the average background photon counts for each individual BATSE GRB light curve, in each of the four main energy channels of BATSE LADs. We then subtract the calculated average background gamma-ray photon counts from the corresponding BATSE GRB light curves. The background-subtracted light curves are then used to calculate the peak photon fluxes of all GRBs in the sample, in three 64, 256, and 1024-ms time-scale definitions. Although the calculated peak fluxes are already contaminated and biased by background noise, we assume they represent the 'true peak fluxes' of BATSE GRBs and use them as our reference to simulate and investigate the effects of background noise in the calculation of peak flux at very low signal-to-noise ratios (SNR). To do so, we add synthetic background noise to the entire time-bins of each of the background-subtracted light

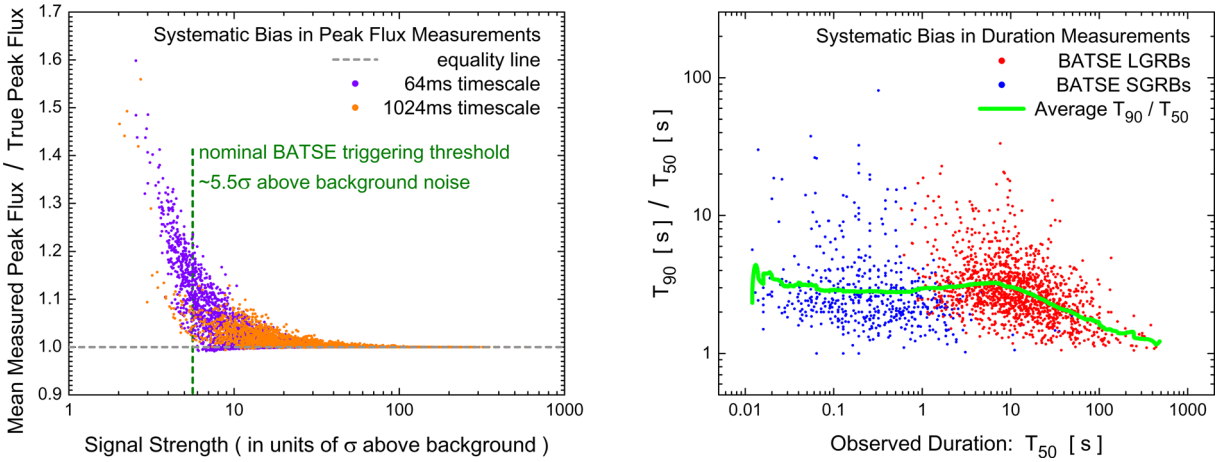

Figure B1. Left: an illustration of the existing systematic bias in the peak flux measurements of BATSE GRBs and possibly other GRB catalogues, such as *Swift* BAT and *Fermi* GBM. The horizontal axis represents the *peak-flux* signal strength of a given BATSE GRB light curve, in units of the standard deviation (σ) of the background photon counts fluctuations. For comparison, the nominal BATSE triggering threshold is shown by the green vertical dashed line. Right: an illustration of the existing systematic bias in the duration measurements of BATSE GRBs, in particular T_{90} definition at very long durations. At durations longer than $T_{90} \sim 30$[s] corresponding to $T_{50} \sim 10$[s] close to detection threshold, the prompt durations of most GRBs tend to be systematically underestimated in BATSE catalogue (cf. Koshut et al. 1996; Hakkila et al. 2000b). This systematic bias is also evident in the top-left and centre-left plots of both Figs 5 and 6.

curves. The noise count (n) for each time-bin in a given GRB light curve is drawn from the Poisson distribution,

$$P(n|\lambda) = \frac{\lambda^n}{n!}\mathrm{e}^{-\lambda}. \quad \text{(B1)}$$

The mean of the noise count (λ) for each BATSE GRB light curve is set to the original mean background photon counts found in each of the original light curves. We then subtract the average background counts (λ) from the newly obtained light curves and measure the new peak fluxes in three time-scales 64, 256, and 1024 ms. This procedure of adding and subtracting synthetic background noise is then repeated 10 000 time for each GRB light curve to obtain a sample of peak flux measurements for each of BATSE catalogue GRB. The mean of this sample is then compared to the original 'true peak flux' measured after the initial background subtraction. The results are illustrated in the *left-hand* plot of Fig. B1. It is evident that peak the flux estimates become increasingly biased with decreasing SNR in BATSE data. This result corroborates the findings of Hogg & Turner (1998), who argue that flux measurements in astronomical surveys tend to be overestimated at very low SNR.

We have also tested the BATSE fluence and spectral peak energy data for the potential existence of systematic biases at low SNR, for which we find no significant evidence. We identify, however, a systematic bias in the duration measurements of BATSE catalogue GRBs, specifically, in very long T_{90} measurements. This is illustrated in the *right-hand* plot of Fig. B1, where we show that the T_{90} measures of BATSE LGRBs are likely systematically underestimated at very long durations, corresponding to durations $T_{50} \gtrsim 10$ [s]. As argued by Koshut et al. (1996), Hakkila et al. (2000b), and Kocevski (2012a), the T_{90} definition of GRB duration seems to be prone to systematic underestimations for very long duration low-SNR GRBs, since it is more likely that the late-time weak signals in the light curves would vanish in the background noise. The effects of this duration bias are also evident in the predictions of the LGRB world model shown in Figs 5 and 6 (*top-left and centre-left* plots in both figures).

This paper has been typeset from a TEX/LATEX file prepared by the author.